

1 **Comparison of Global Precipitation Estimates across a Range of Temporal**
2 **and Spatial Scales**

3 Maria Gehne*

4 *CIRES, University of Colorado, Boulder, Colorado*

5 Thomas M. Hamill

6 *NOAA Earth System Research Laboratory, Physical Sciences Division, Boulder, Colorado*

7 George N. Kiladis

8 *NOAA Earth System Research Laboratory, Physical Sciences Division, Boulder, Colorado*

9 Kevin E. Trenberth

10 *National Center for Atmospheric Research, Boulder, Colorado*

11 *Corresponding author address: CIRES, University of Colorado, Boulder, Colorado.

12 E-mail: maria.gehne@noaa.gov

ABSTRACT

13 Characteristics of precipitation estimates for rate and amount from three
14 global High-resolution precipitation products (HRPPs), four global Climate
15 Data Records, and four reanalyses are compared here. All data sets consid-
16 ered have at least daily temporal resolution. Estimates of global precipitation
17 differ widely from one product to the next, with some differences likely due to
18 differing goals in producing the estimates. HRPPs are intended to produce the
19 best instantaneous precipitation estimate locally. Climate data records of pre-
20 cipitation emphasize homogeneity over instantaneous accuracy. Precipitation
21 estimates from global reanalyses are dynamically consistent with the large
22 scale circulation but tend to compare poorly to rain gauge estimates as they
23 are forecast by the reanalysis system and precipitation is not assimilated. As
24 expected, variance and the average spread among data sets are highest where
25 the means are large. Regionally, differences in the means and variances are
26 as large as the means and variances respectively. Temporal correlation, rain
27 rate and rain amount distributions, and biases in time evolution are explored
28 using temporal and spatial averaging. It is shown that differences on annual
29 time scales and continental regions are around 0.8mm/d, which correspond to
30 $23W m^{-2}$. These wide variations in the estimates, even for global averages,
31 highlight the need for better constrained precipitation products in the future.

32 **1. Introduction**

33 Gridded estimates of daily (or higher frequency) global precipitation are becoming more and
34 more necessary for applications such as model validation, input for land-surface models, or
35 extreme-event characterization. Detailed knowledge about current precipitation distributions is
36 also necessary to quantify changes in precipitation estimated by global-warming scenarios, which
37 tend to be described as changes in the mean and tails of the distribution. All of these applications
38 assume that an accurate or at least adequate estimate of these distributions is obtainable.

39 Because there is a strong connection between temporal and spatial variability of precipitation,
40 and variability of precipitation decreases with both longer time and larger spatial averages (Bell
41 et al. 1990), what is adequate depends on the application. On monthly scales global precipitation
42 estimates have been used to estimate the global water cycle (Trenberth et al. 2007; Rodell et al.
43 2015), study the co-variability of precipitation and surface temperature (Trenberth and Shea 2005),
44 and to assess the imbalance between global precipitation and evaporation (Schlosser and Houser
45 2007; Trenberth and Fasullo 2013). Datasets that are able to resolve monthly variability and
46 continental scales are suitable for estimates of the global water cycle. For many other applications,
47 higher temporal (sub-monthly) and spatial resolution is needed. Validation of model forecast
48 precipitation needs data sets with similar or higher resolution to the model output which can range
49 from a few kilometers to 1° and 1h to daily depending on the model used (Hamill 2012; Brown
50 et al. 2012; Lindvall et al. 2013). For example, hourly resolution sets a good compromise between
51 what is meaningful in models and useful for extremes. Station data are also used, but this approach
52 depends on a high enough station density in the verification region (Gutowski Jr. et al. 2003). One
53 of the major outputs of land-surface models, soil moisture, is highly variable in space and spatial
54 patterns depend strongly on the precipitation forcing the model even down to a resolution of 2km

55 (McLaughlin et al. 2006). In general, for land-surface models at coarser resolutions (e.g. T382)
56 hourly precipitation data are given as input and interpolated to the model time step of 15 or 20
57 minutes (Liu et al. 2011; Meng et al. 2012). Observed extreme precipitation events are usually
58 highly localized in space and time, involving scales on the order of minutes to a few hours and
59 several kilometers, especially in the tropics and during summer over land. To resolve the more
60 extreme precipitation intensity events and accurately estimate the tails of the distribution, data at
61 a resolution of ten minute intervals and about 1km thus might be needed (Haerter et al. 2010). To
62 accurately identify the mean diurnal cycle, hourly time steps are desirable to resolve the evolution
63 of precipitation throughout the day.

64 Estimates of precipitation from individual rain-gauges exist in many locations, but these are
65 point estimates and apply only for the location they were collected. Gridded rain-gauge based
66 analyses of precipitation are available over the global land areas, with the estimates assumed to be
67 representative for a given area. However, large land and especially oceanic areas on the globe are
68 very sparsely covered with rain gauges. This is problematic, because in sparsely sampled areas,
69 interpolation between rain gauge locations to obtain a gridded analysis will introduce errors. In
70 addition, rain-gauge estimates are thought to underestimate precipitation rates due to under-catch
71 in windy or snow conditions (e.g. Peterson et al. 1998; Adam and Lettenmaier 2003). Another
72 issue is that precipitation measurements are usually reported only once or twice a day, which af-
73 fects the resolution of both rates and totals, because the longer the precipitation is left in the gauge
74 the greater the potential for some of it to evaporate. However, as noted above, resolving the very
75 high rates in thunderstorms requires temporal resolution of hours or even minutes. Overall, gauge-
76 based analyses are likely to be quite accurate in data-dense areas and questionable in data-sparse
77 areas. Other available options for global precipitation estimates, that provide higher spatial and
78 temporal resolution, are based on satellite data. The highest resolutions of current global pre-

79 precipitation estimates are 3 hours and 0.25° . While there are versions of some of these data sets
80 available at higher resolutions, on a global scale data handling can become an issue. Data at 3
81 hours and 0.25° is marginally adequate to resolve the diurnal cycle and mesoscale systems but
82 is still too coarse to resolve individual convective extreme events. Most satellite based data sets
83 have time series of less than 15 years (with one recent exception, see section 2), which is not long
84 enough to estimate trends or a robust climatology. Precipitation estimates from satellite retrievals
85 are inferred from infrared (IR) or microwave (MW) measurements rather than measured directly.
86 IR measurements, which tend to be from geostationary satellites have high spatial and temporal
87 resolution, while MW or radar measurements are obtained from polar orbiting satellites with much
88 sparser sampling (Wolff and Fisher 2008). Global reanalyses offer another way to estimate global
89 precipitation with the advantage that they synthesize many different data sources. However, while
90 the underlying dynamical model is dynamically consistent, adjustments to assimilated data result
91 in a product that is not necessarily mass or energy conserving. Precipitation in particular is typi-
92 cally the preservation of the previous forecast cycle's guess, which is contaminated by model bias.
93 In addition, the spatial resolution is limited to that of the reanalysis.

94 There are several important questions users of these data sets need to ask. The most important
95 one is obviously, which of these estimates is closest to the truth? There is no clear answer to
96 this question. The conclusion of several precipitation inter-comparison projects was that no one
97 methodology is superior to the others (Kidd and Huffman 2011). In an early study Smith et al.
98 (1998) showed that for regional comparisons, uncertainty in the ground validation data can be
99 larger than the passive microwave (PMW) algorithm bias in many cases. They also showed that the
100 differences in estimated rain rates are mainly due to how the more intense rain rates are calculated
101 and how strict the screen (precipitating versus dry pixels) is.

102 On monthly timescales for global analyses, Adler et al. (2001) show that merged analysis prod-
103 ucts, using more than one satellite source and adjusted to rain gauges, are superior to single source
104 products. Without the adjustment to rain gauges, large biases exist over the southern Great Plains
105 in the US for high resolution precipitation products (Sapiano and Arkin 2009). Even rain gauge-
106 only data sets have large differences; in the context of drought, using one or another data set can
107 result in an increase or decrease in the determination of drought conditions (Trenberth et al. 2014).
108 The main conclusion from these studies is that there is no one best product, there is only the most
109 appropriate product for a certain purpose. For example, studies at different locations and different
110 seasons will likely benefit from using the product that has been shown to do well under those con-
111 ditions. If the emphasis is on consistency of precipitation with circulation patterns, then reanalysis
112 products combined with observed precipitation may be the best choice. In addition, several other
113 issues are not addressed in these previous studies, such as whether there are systematic biases
114 among the high-resolution precipitation estimates on the global scale? In all cases it is important
115 for the user to know how the products differ systematically in their precipitation estimates. In order
116 to answer this question it is necessary to first quantify the differences among the data sets and the
117 different estimation approaches. Are there biases particular to a certain approach to precipitation
118 estimation? How do the distributions differ? And, given all the different estimates, is there a way
119 to quantify the uncertainty associated with them? In terms of length of time series, studies that
120 deal with multi-annual assessment of precipitation are rare (Prat and Nelson 2015), which is why
121 we focus on data sets with more than 10 years of overlap. And while there are plenty of local and
122 regional comparisons between and validation of data sets (e.g. Gutowski Jr. et al. 2003; Sohn et al.
123 2010; Kidd et al. 2012), here we focus on global products.

124 The aim of this study, is not to determine which data set is closest to the absolute truth, since
125 that is impossible, but rather to identify strengths and shortcomings of the data sets, and to provide

126 some guidance as to which data sets are likely to perform better in certain situations. We are
127 interested in global precipitation data sets with daily or higher resolution. Since distributions
128 of precipitation are highly dependent on the resolution of the data used to compute them, daily
129 or higher temporal resolution is better suited for estimating distributions than monthly resolution.
130 The larger sample size and range of precipitation rates resolved by daily data lead to more accurate
131 representation of the distributions.

132 Section 2 introduces the data sets used in this study. Section 3 has the details of the statistics used
133 to compare the precipitation estimates and how the distributions are computed. Section 4 evaluates
134 the statistics and distributions, mostly on the example of North America, but other continental
135 regions are mentioned to highlight stark differences or close similarities. Figures for all other
136 continental regions are included in the supplementary material. Lastly, section 5 summarizes and
137 discusses the implications of the results presented in this study.

138 **2. Data Sets**

139 The lowest native resolution of all precipitation data sets under consideration here is daily on a
140 1° grid. Therefore, all data sets were interpolated from their original grids to a grid with 1° spatial
141 and daily temporal resolution using conservative averaging. This was done to facilitate comparison
142 of distributions and variability, to ensure that the precipitation estimates are comparable and to
143 minimize differences among the data sets due to differing resolutions. As temporal averaging is
144 done to daily resolution, differences in the diurnal cycle phase and amplitude will not be resolved;
145 the resolved time scales that will be considered are daily to interannual. The seasonal cycle has a
146 large effect on precipitation, so all analyses are performed for each month of the year separately.

147 Our criteria (global data, daily resolution) exclude several well established precipitation esti-
148 mates from this study, for reasons related to either their temporal resolution or their regional cover-

149 age. These include PRISM (Daly et al. 1994), the North American regional reanalysis (Mesinger
150 et al. 2006), stage IV radar data (Lin and Mitchell 2005), and Asian Precipitation - Highly Re-
151 solved Observational Data Integration Towards Evaluation of Water Resources (APHRODITE,
152 Yatagai et al. 2012), because they are regional products, and the Global Precipitation Climatology
153 Centre (GPCC, Becker et al. 2013), GPCP monthly estimates (Huffman et al. 1997), CPC merged
154 analysis of precipitation (CMAP, Xie and Arkin 1997) and CRU precipitation (Harris et al. 2014),
155 because of their monthly resolution.

156 *a. High-resolution precipitation products*

157 High-resolution precipitation products (HRPPs) aim to provide the best instantaneous precipi-
158 tation estimates at high spatial and temporal resolution. Commonly, high-resolution infrared (IR)
159 brightness temperatures from geostationary satellites are related to precipitation rates using the
160 more accurate passive microwave (PMW) estimates from the polar-orbiting satellites. How these
161 measurements are related, how the IR is calibrated, and whether the monthly means are scaled to
162 match monthly rain gauge analyses varies between algorithms and constitutes the main sources
163 of differences between the estimates; see Kidd and Huffman (2011) for an overview and an in-
164 depth description of the various techniques. In general, PMW gives a more accurate estimate of
165 precipitation than IR, because of the more direct observation of precipitation. But this accuracy
166 deteriorates for time averages due to the lower sampling frequency of PMW compared to IR. The
167 combination of PMW and IR measurements includes the different errors inherent in each tech-
168 nique (Kidd and Huffman 2011). We note, that there are versions of these precipitation products
169 with higher resolutions than used here. However, a higher resolution would not be advantageous
170 for the analysis presented here, since all data sets need to be interpolated to match the lowest
171 resolution data set available.

172 The Climate Prediction Center morphing method (CMORPHv0.x, Joyce et al. (2004); Joyce
173 and Janowiak (2005)) estimates rainfall by combining IR and PMW measurements. High-quality
174 PMW rainfall estimates are propagated (using linear interpolation in time) by motion vectors de-
175 rived from high frequency IR imagery. CMORPH is available from 2003-2013 at 3-hourly inter-
176 vals on a 0.25° grid from 60°S to 60°N . A bias corrected version (CMORPHCRTv1.0, Joyce et al.
177 (2004); CMORPHv1.0 (2015)) is also available on the same grid, from 1998-2013. CMORPHCRT
178 uses a constant algorithm and is bias corrected against a rain gauge analysis over land and GPCP
179 pentad data over the ocean. Correction over land is done by PDF matching against daily gauge
180 analysis using optimal interpolation with orographic correction. The bias correction results in a
181 reduction of the spurious trends seen in CMORPH. For better visualization, results are shown for
182 CMORPHCRT only and results for CMORPH are mentioned where appropriate. Both products
183 are also available at a resolution of 8km and 30min, but the higher resolution is not necessary for
184 the analysis presented here.

185 The Tropical Rainfall Measuring Mission (TRMM) 3B42v7 product, provides 3-hourly precip-
186 itation estimates on a 0.25° grid between 50°S to 50°N and from 1998 to 2013. The monthly
187 means of the 3-hourly microwave-calibrated IR rainfall estimates are combined with the Global
188 Precipitation Climatology Centre (GPCC) monthly rain-gauge analysis to generate a monthly
189 satellite-gauge combination (TRMM3B43). Each 3-hourly field is then scaled by the correspond-
190 ing monthly satellite-gauge field. Like all satellite precipitation estimates, TRMM was previously
191 determined to have large relative errors at small precipitation rates, however time/area averaging
192 significantly reduces the random error (Huffman et al. 2007, 2012).

193 The Precipitation Estimation from Remotely Sensed Information using Artificial Neural Net-
194 works (PERSIANN) algorithm merges high-frequency IR images with low frequency rainfall esti-
195 mates from the TRMM satellite using artificial neural networks (Hsu et al. 1997; Sorooshian et al.

196 2000; Braithwaite 2000). The precipitation estimates are based on IR from geostationary satellites,
197 and PMW measurements are used to update the algorithm parameters. PERSIANN is available
198 from 2001-2013 at 3-hourly intervals on a 0.25° grid from 50°S to 50°N .

199 *b. Climate data records of precipitation*

200 For climate data records homogeneity is emphasized over instantaneous accuracy. The Climate
201 Prediction Center (CPC) rain-gauge (GAUGE) data set is based on quality-controlled station data
202 from more than 30000 stations. These data are then interpolated to create analyzed fields of daily
203 precipitation with bias correction for orographic effects (Xie et al. 2007). The global analysis
204 is available daily on a 0.5° grid from 1979-2005 (Xie et al. 2007; Chen et al. 2008; Xie 2009).
205 The real-time version of the CPC gauge data set (GAUGERT) uses about 17000 stations and is
206 available on the same grid at the same time resolution from 2005-2013. Large scale averages
207 of long term means and variances are comparable between GAUGE and GAUGERT. Additional
208 stations used in the GAUGE estimate are generally located in regions of dense observing networks.
209 In regions with sparse observations the number of stations stays about the same from GAUGE to
210 GAUGERT. Because of this GAUGE and GAUGERT estimates are combined by extending the
211 GAUGE data with the GAUGERT data and the resulting data set is referred to as GAUGE+RT.

212 Global Precipitation Climatology Project (GPCP1DD, v1.2) daily, 1° precipitation estimates
213 between 40°S - 40°N are computed based on the threshold-matched precipitation index (TMPI)
214 (Huffman et al. 2000). Outside of that, the developers use an adjusted Susskind TOVS/AIRS cloud
215 volume proxy. For the TMPI, IR temperatures are compared to a threshold, and all cold pixels are
216 given the same conditional precipitation rate, with threshold and conditional precipitation rate set
217 locally by month. GPCP1DD monthly means are normalized to match the monthly GPCP satellite-
218 gauge precipitation estimate version 2.2 (Adler et al. 2003), which is based on satellite data and

219 rain-gauge analysis from the GPCC. The GPCC monthly rain gauge analysis is bias corrected
220 to account for systematic errors due to wetting, evaporation, or aerodynamic effects (Huffman
221 et al. 1997). The GPCP1DD daily, 1° precipitation estimates are available on a global grid from
222 1996-present (Bolvin 2001).

223 One of the latest climate data records is the Precipitation Estimation from Remotely Sensed
224 Information using Artificial Neural Networks - Climate Data Record (PERSICDR, v1r1, Ashouri
225 et al. 2015; Sorooshian et al. 2014). This is generated using the PERSIANN algorithm, and ad-
226 justed using the GPCP1DD monthly product to match monthly precipitation rates on a 2.5° grid
227 between the two products. In contrast to the HRPP PERSIANN, the PERSICDR model is pre-
228 trained on stage IV hourly precipitation data and the model parameters are then kept fixed for the
229 full historical record of IR data. PERSICDR is available on a 0.25° grid between 50°S to 50°N
230 and from 1983 to present day.

231 *c. Reanalysis precipitation products*

232 Another way to estimate global precipitation is through short-term forecasts provided by global
233 reanalyses. The underlying models assimilate a wide variety of observations, but in general not
234 precipitation measurements or analyses. Precipitation is usually provided by a prior short-range
235 forecast, and this inherits the systematic errors of the forecast model. The advantage to reanalyses
236 is that all variables are somewhat dynamically consistent. While the underlying dynamical model
237 is dynamically consistent, adjustments to assimilated data result in a product that is not necessarily
238 mass or energy conserving. However, as precipitation data are not typically constrained by the
239 analysis procedure, reanalyzed precipitation is highly model dependent (Trenberth et al. 2011).
240 This is particularly true in the tropics and over continents during the summer, when convective
241 precipitation dominates. This leads to the well-known problem with precipitation estimates from

242 general circulation models (GCMs) of raining too frequently, with an over-abundance of light
243 rainfall and too infrequent extreme precipitation (e.g. Trenberth et al. 2003; Wilcox and Donner
244 2007; Stephens et al. 2010). As global reanalyses are based on similar GCMs they tend to have
245 the same short-comings in this respect. One exception is the North American Regional Reanalysis
246 (Mesinger et al. 2006), which does assimilate precipitation. And there is evidence that assimilation
247 of precipitation significantly improves precipitation estimates and the atmospheric moisture budget
248 (Ruane 2010a,b; Kennedy et al. 2011) and the forecast of other variables (Lien et al. 2015).

249 The decrease of precipitation variability with spatial averaging implies that to facilitate compar-
250 ison of reanalyses with the other precipitation estimates, the reanalyses must be generated at as
251 high a resolution as the other estimates. Lower-resolution reanalyses previously have been found
252 to have lower rain rates and a smaller range of resolved rain rates overall as compared to satellite
253 or gauge based estimates, similar to operational forecast models (Janowiak et al. 2010). This is
254 valid even when area averaging (and thus decreasing the variability of) the observational estimates
255 to the same resolution as the reanalyses. We obtained similar results when applying our analysis
256 to lower resolution reanalyses. In addition, reanalyses are based on GCMs and their parameteri-
257 zations and therefore have a similar problem as the GCMs which tend to precipitate lightly almost
258 constantly. Here we consider the most recent global reanalyses products which have a spatial res-
259 olution of smaller than 1° . They are the European Centre for Medium-Range Weather Forecast-
260 ing (ECMWF) ERA-Interim reanalysis (ERA-Interim Dee et al. 2011a,b), the Modern-Era Retrospective
261 Analysis for Research and Applications (MERRA Rienecker et al. 2011a,b), MERRA Version 2
262 (MERRA2 Bosilovich et al. 2015a,b), the NCEP Climate Forecast System Reanalysis (CFSR Saha
263 et al. 2010a,b), and the Japanese 55-year Reanalysis (JRA55 Kobayashi et al. 2015b,a).

264 *d. Caveat to independence of precipitation estimates*

265 None of the above precipitation estimates is independent of all the others, for there is a large
266 degree of overlap in the source data that goes into the different estimates (Table 1). PERSIANN
267 and CMORPH are the only satellite products without routine inclusion of gauge data. Both TRMM
268 and GPCP1DD use the same monthly satellite-gauge combination algorithm (Huffman et al. 1997)
269 to constrain their monthly totals. As mentioned above, the GAUGE and GAUGERT estimates are
270 for non-overlapping time periods and use a different total number of stations, but the underlying
271 algorithm is the same. Their statistics compare very well even though only about half the number
272 of stations are available for the real-time product GAUGERT (17000 compared to 30000 for the
273 retrospective GAUGE analysis).

274 **3. Methods**

275 The first step, before any other analysis is done, is to interpolate all data sets from their original
276 grids to a coarser grid with 1° spatial and daily temporal resolution using conservative averaging.
277 GPCP1DD has the coarsest resolution in both time and space at 1° , daily resolution, and all other
278 data sets are interpolated to the same grid. All results shown and all computations are done on the
279 regrided data sets in an attempt to minimize the impacts of differing resolution on the results.

280 The methods used to evaluate the precipitation estimates include basic statistical quantities such
281 as means and variances, and their differences among products at each grid point (Table 2). We also
282 show the mean and variance differences as percentage of the mean and variance respectively to
283 compare their relative sizes. In addition we consider temporal averages on time scales of a week,
284 a month and a year. Spatial averages are always area averages, taking into account the change in
285 grid area with latitude.

286 Frequency distributions of precipitation are highly skewed, with the smallest rain rates being the
287 most frequent. In general this makes comparing different distributions difficult, because the tails
288 tend to be under-sampled. One way to reduce the discrepancy between the number of samples in
289 the lower rain rate bins and the higher rain rate bins is to use logarithmic bin sizes that increase with
290 rain rate. Of course, in that case care needs to be taken when computing integrals. In addition to
291 frequency distributions of precipitation rate we also compare rain amount by rain rate distributions.
292 The integral under the curve is equal to the total precipitation amount. These distributions tend
293 to be skewed towards lower precipitation rates with the largest amounts occurring at intermediate
294 rain rates. For both types of distributions a logarithmic bin size is used. The number of bins is
295 100 with a constant logarithmic (to base 10) bin length. Setting the minimum bin to 10^{-4} and
296 the maximum to 10, the bin length then comes out to $\Delta b = (\log_{10} 10 - \log_{10} 10^{-4}) / 100 = 0.05$.
297 The edges of the bins are computed according to $b_i = 10^{-4} 10^{i\Delta b}, i = 0, \dots, 100$, which results in
298 increasing bin sizes with precipitation rate. Rain rates below the minimum (including zero rain
299 rates) are counted in the lowest bin.

300 Global maps of the spread among precipitation data sets (Table 2) can be used to identify regions
301 with more or less variability among the data sets. First the mean seasonal cycle is removed from
302 each data set. The spread is then computed as the standard deviation among data sets at each grid
303 point and time and averaged for each month of the year.

304 4. Results

305 The continental regions used in the analyses are defined as the land areas contained within the
306 latitude-longitude areas given in Table 3. All results presented are for data interpolated to match
307 the GPCP1DD 1° , daily resolution.

308 *a. Annual cycle*

309 A summary of the annual cycle is given in Figs. 1 and 2 in form of its amplitude and phase. The
310 annual cycle is defined as the first 4 harmonics of the mean daily seasonal cycle. Differences in
311 the amplitude are large over equatorial Africa and South America, and the Indian Monsoon region.
312 Over North America the amplitude of the annual cycle in the Midwest of the United States ranges
313 between 3 – 13mm d⁻¹. The phase is defined as the day of the year the annual cycle is maximized,
314 and so does not take into account if a location has multiple maxima in precipitation during the year.
315 This is potentially an issue in equatorial South America and Africa, although overall the timing of
316 the reported annual maxima in precipitation is captured consistently among the estimates. Regions
317 with large discrepancies in timing are northern Africa, parts of Australia (both regions where the
318 annual cycle amplitude is very small), and the northwestern United States (Fig. 2).

319 *b. Differences in means and variances*

320 To compare patterns of monthly means and variances it was necessary to choose one of the data
321 sets to compare with the others. We chose GPCP1DD, not because it is the most accurate daily
322 precipitation estimate, but because it is widely used and readers may have more familiarity with
323 GPCP1DD than other data sets. GPCP1DD also has the most extensive time coverage except for
324 PERSICDR, which is a newer product. In addition, GPCP1DD is the only precipitation estimate
325 that is truly global.

326 Distinctive differences among data sets of large-scale patterns of means and variances can be
327 identified. The climatological mean monthly precipitation for July is shown in Fig. 4. Comparison
328 of the mean monthly precipitation across data sets shows large variability (Fig. 4b-d), especially
329 in areas like the Intertropical convergence zone (ITCZ). Other regions with large differences in the
330 means are continental areas in the summer hemisphere and the western boundary ocean current

331 regions. Because of large spatial gradients in some regions, small variations in the location of
332 climatological features like the ITCZ can lead to large local differences in mean precipitation.

333 Figures 4c,d and 5c,d show that GPCP1DD mean precipitation exceeds mean precipitation from
334 satellite-only product PERSIANN and over the oceans, except in regions with intense convective
335 precipitation. The bias corrected CMORPHCRT has small differences to GPCP1DD compara-
336 ble to GAUGE+RT. In particular, CMORPHCRT exceeds GPCP1DD over tropical oceans, and
337 GPCP1DD exceeds CMORPHCRT over tropical land areas and over the midlatitudes in winter.
338 As is to be expected based on previous work, TRMM and GPCP1DD match well over land, but
339 TRMM commonly has higher means over tropical oceans and smaller means over midlatitude
340 ocean areas (Fig. 4b). The closest match is between GPCP1DD and PERSICDR monthly means
341 (Fig. 4f), where any differences are below 0.075mm d^{-1} . This is to be expected based on the
342 construction of GPCP1DD and PERSICDR. Satellite-only product PERSIANN has higher means
343 over summertime continental regions than the gauge corrected estimates. Over land the main bias
344 for gauge-corrected precipitation estimates is due to the bias in the rain gauge analysis used. This
345 is visible in the differences between GPCP1DD monthly means and GAUGE+RT monthly means
346 (Figs. 4e and 5e), where the rain gauge analysis that contributes to GPCP1DD is bias corrected for
347 losses due to wetting, evaporation, or aerodynamic effects, and the CPC GAUGE+RT analysis is
348 corrected for orographic effects. Comparing the July estimates to January it becomes clear that and
349 PERSIANN tends to underestimate winter precipitation over continents and overestimate summer
350 precipitation when compared to GPCP1DD. GAUGE+RT estimates are biased low on average, but
351 not everywhere compared to GPCP1DD, and TRMM exceeds GPCP1DD in regions of vigorous
352 convection.

353 Percentage differences of the monthly means (Fig. 6) show clearly that the differences in the
354 means are often as large as the means. This is especially true in areas with small mean values

355 like the subtropical dry zones, where small differences translate into large percentage differences.
356 Depending on the data set under consideration, this can also be the case in regions with large mean
357 precipitation and large variability like the continental US in the summer and the edge of the ITCZ
358 (e.g. GPCP1DD and PERSIANN (Fig. 6d)).

359 Monthly mean daily precipitation variance is large where mean precipitation is large (Figs. 4a
360 and 7a). The largest variances are in areas with highly variable convective precipitation such as
361 the ITCZ, the Indian Ocean, and the Indian Monsoon region. TRMM and CMORPHCRT have the
362 largest variance on average (Fig. 7b,c), and differences in variances are as large as the variance
363 for most areas of the globe (not shown). This holds even for areas with large variability, like
364 the ITCZ. That magnitudes of spread and mean should correlate is to be expected for a positive
365 definite quantity like precipitation, but the magnitude of the difference in variance among data sets
366 is notable. The combined rain gauge data set GAUGE+RT shows smaller variance than GPCP1DD
367 (Fig. 7e and 8e) over boreal winter land areas and the opposite during boreal summer. Results
368 are more mixed over South America, Africa and Australia. PERSICDR variance is smaller than
369 GPCP1DD variance over land, but exceeds GPCP1DD variance over the ocean. Note, however,
370 that differences in variance are smaller between PERSICDR and GPCP1DD than for any other
371 data set Fig. 7f and 8f). While small differences between the means of PERSICDR and GPCP1DD
372 are to be expected, that expectation does not hold for daily variance. While CMORPHCRT has
373 the larger variance for most regions, Figs. 7c and 8c show that GPCP1DD variance is higher in
374 the winter hemisphere.

375 *c. Time Series*

376 Next, we examine time series at the continental scale for North America, where there is a rela-
377 tively dense observing network and so the potential for constraining estimates is high. Time series

378 averaged over North America are also a good example in that they illustrate many of the issues
379 also observed in other regions. Other regions (Table 3) are mentioned where results are notable,
380 but results are not shown. Figures for all other regions are included in the supplementary material.
381 Figure 3 and Table 3 also include the amplitude and phase of the mean seasonal cycle averaged
382 over each continental region. The minimum and maximum amplitude estimated by the different
383 products in general differ by a factor of 1.5 – 3. The timing of the seasonal cycle is estimated
384 within 30 days for North America, Asia, Australia and the maritime continent, but for Europe the
385 estimates differ by 46 days. Note that the outliers for the timing are not necessarily the reanalyses.
386 For North America it is GAUGE+RT and for Europe it is PERSIANN that place the maximum
387 of the annual cycle earlier in the year than the other estimates. South America and Africa have
388 two maxima in the seasonal cycle, and there is disagreement among data sets on which maximum
389 dominates.

390 The temporal evolution of global land-averaged precipitation rates on annual and monthly
391 timescales are shown in Fig. 9. The interannual variability that can be seen in the annual
392 means is somewhat consistent among most data sets, although there appears to be an offset of
393 $0.5 - 1\text{mm d}^{-1}$ between the estimates (Fig. 9a), this decreases to 0.3mm d^{-1} when anomalies
394 from the seasonal cycle are considered (not shown). The outliers for annual averages are PER-
395 SIANN and to a lesser degree MERRA2 and CFSR. CFSR appears to have a positive trend from
396 2001 to 2010 not seen in the other estimates; this trend is mostly due to trends over South Amer-
397 ica and Africa (not shown) and can be related to the changing observing system (Trenberth et al.
398 2011). Previous studies have shown that precipitation from reanalyses that assimilate moisture
399 from satellite observations are strongly affected by changes in the observing system and result
400 in spurious trends in the precipitation estimates (Trenberth et al. 2011). PERSIANN has anoma-
401 lously high rain rates from late 2006 to early 2007 and anomalously low rate in late 2005 and early

402 2008 (Fig. 9b). Over the global ocean the differences among annual averages are larger, up to
403 2mm d^{-1} , and the reanalyses have a small but significant upward trend not seen in the GPCP1DD,
404 PERSICDR and TRMM estimates (not shown). PERSIANN in contrast has a negative trend over
405 the ocean.

406 The timing of the seasonal cycle over North America is captured more or less consistently by
407 all estimates (Fig. 10b), but the amplitude is not. CMORPHCRT and PERSIANN underestimate
408 winter precipitation rates relative to other analyses by up to 1mm d^{-1} on monthly time scales,
409 while ERAI under-estimates summer precipitation rates. On weekly time scales the differences
410 can be as large as 3mm d^{-1} in the winter, with PERSIANN estimating $< 0.5\text{mm d}^{-1}$ and all other
411 estimates averaging between $2.5 - 3\text{mm d}^{-1}$ (Fig. 10c). This large difference illustrates a known
412 issue with PERSIANN and other satellite-only products. Several studies have shown that winter-
413 time precipitation is severely underestimated in these products for different regions in the northern
414 midlatitudes (Sapiano and Arkin 2009; Sohn et al. 2010; Kidd et al. 2012). Relative differences
415 over North America in the summer are of the same order as over the maritime continent, even
416 though total amounts are much larger over the maritime continent.

417 To assess the consistency of the time evolution among the data sets, we consider correlations on
418 annual, monthly and daily time scales with GPCP1DD and GAUGE+RT. One note of caution is
419 necessary for interpreting the annual time scale results. The time series of annual means only have
420 12 data points from 2001-2012. This severely limits the sample size and leads to unstable estimates
421 of the correlations on annual time scales. We show results for correlation with GPCP1DD only,
422 but mention how these compare with correlations with GAUGE+RT. Correlations of the time se-
423 ries of continental mean precipitation anomalies with GPCP1DD reveal large positive correlations
424 on annual, monthly and daily time scales for some data sets, TRMM and PERSICDR in particular
425 (Table 4). For other data sets the correlations were generally not significantly different from zero

426 on annual and daily timescales (e.g. PERSIANN), but were on monthly time scales. Low corre-
427 lation for annual averages indicate potential long-term differences in the continental scale water
428 budgets associated with the different data sets that would need to be balanced by evaporation or
429 runoff. Results for reanalyses are mixed. Correlations on annual timescales are not significant for
430 3 reanalyses over North America (JRA55,CFSR and ERAI), but > 0.79 for all reanalyses over Eu-
431 rope, the maritime continent (except MERRA2) and Australia. Meanwhile, correlations are fairly
432 high for both monthly and daily timescales. Comparison of correlations with GAUGE+RT instead
433 of GPCP1DD (not shown) reveal that for North America on annual time scales all data sets ex-
434 cept PERSIANN have correlations higher than 0.8 with GAUGE+RT. Over Europe data sets with
435 higher correlation with GPCP1DD are TRMM, PERSICDR, MERRA and ERAI, data sets with
436 higher correlation with GAUGE+RT are CMORPHCRT, MERRA2 and CFSR. On monthly time
437 scales both CMORPHCRT and MERRA2 correlate better with GAUGE+RT, while all other data
438 sets correlate better with GPCP1DD. For daily data correlations between GPCP1DD and all other
439 data sets are higher than for GAUGE+RT, with the exception of the reanalyses over Europe.

440 The low correlations of large scale (continental to global) annual averages of precipitation esti-
441 mates indicate that the estimates differ in their interannual variability. Imbalances on these scales
442 in estimates of an important component of the global water cycle affect our ability to close the
443 budget (Trenberth et al. 2007, 2011). Global land differences on annual time scales are about
444 0.8mm d^{-1} for the observational estimates. This translates to differences of up to 23.2W m^{-2} ,
445 which is very large compared to the global land latent heat flux of 38.5W m^{-2} estimated by Tren-
446 berth et al. (2009). Including the reanalyses increases the offset to 1mm d^{-1} .

447 *d. Distributions*

448 In this section, we examine area-averaged seasonal distributions. The general behavior of these
449 distributions is very similar among the continental areas. When plotted on a log-log scale (not
450 shown), the distribution curves have two distinct slopes, positive for low rain rates and negative
451 for higher rain rates. The transition between these slopes is more abrupt in the summer and more
452 gradual in the winter months for North America. For Africa and the maritime continent, the
453 transition is abrupt for all months (not shown). This relationship appears to hold for all continental
454 areas during the summer months when precipitation tends to be in a more convective regime,
455 which leads us to speculate that the manner of transition between slopes could be related to the
456 dominant precipitation regime (large-scale vs. convective). While the location of where the slopes
457 in the log-log plot change is around 0.5mm h^{-1} for all seasons and regions, the slopes are quite
458 variable between months, data sets and regions.

459 Fig. 11 shows the area-averaged seasonal distributions for North America. At the lowest pre-
460 cipitation rates, CMORPHCRT has a positive bias, with lower rain rates being more common than
461 in other reanalyses or observational data sets. This is consistent with all other continental areas
462 except Africa and Australia. This low precipitation rate bias can also be seen in the older ver-
463 sion of CMORPH that has not been bias corrected. Over Australia, ERAI has a high bias at low
464 rain rates in austral summer and PERSIANN in austral winter. ERAI distributions over Australia,
465 Africa and Asia are bimodal, unlike the other precipitation estimates. The bulk of the distribution
466 is between $0.01 - 1\text{mm h}^{-1}$, with the peak in the distribution shifting between 0.015mm h^{-1} in the
467 winter and 0.5mm h^{-1} in the summer for North America (Fig. 11c). In general, reanalyses, and
468 ERAI in particular, dominate the distribution at these rates. For midlatitude continental regions,
469 CMORPHCRT, and PERSIANN to a lesser degree, are a lot less likely than other products to have

470 precipitation occur at the intermediate rates $0.01 - 1 \text{ mm h}^{-1}$. Fig. 12 examines the differences in
471 the tails of the precipitation distributions. Overall reanalyses tend to not produce very high rain
472 rates, with the exception of MERRA2. This could be because of the grid area vs. point estimate,
473 the convective parameterizations used, or the relatively large grid size. For North America in the
474 winter TRMM has the highest rain rates and highest probability of high rates occurring (Fig. 12a).
475 In the summer (Fig. 12c) the satellite-only estimates dominate at the highest rain rates. For other
476 regions MERRA2 dominates the tails in in South America, Africa and the maritime continent (not
477 shown). The satellite-only product, PERSIANN, tends to accentuate the tail of the distribution
478 during summertime convective precipitation regimes. During months when precipitation is dom-
479 inated by synoptic systems or when the ground is covered in snow (e.g. Europe in the winter
480 months) the tails of the distributions of PERSIANN are even lower than the reanalyses.

481 A different way to compare the data sets is through the distribution of the rain amount by rain
482 rate (Fig. 13). Precipitation amount distributions tend to be skewed in a logarithmic plot, with a
483 long tail towards lower rain rates. Rain rates below 0.01 mm h^{-1} are very common, but the actual
484 rain amount from precipitation at these rates does not add up to much. During the winter months
485 (Fig. 13a), the distributions for CMORPHCRT and PERSIANN are much flatter, and the mean
486 total precipitation amount of CMORPHCRT in DJF is 29mm, whereas it is 56mm for GPCP1DD
487 and 66mm for CFSR. That is a difference of more than 200% for the mean seasonal total estimate.
488 Excluding CFSR which has been shown to overestimate moisture transport from ocean to land
489 and where at least some of the precipitation over land is due to the analysis increment (Trenberth
490 et al. 2011), there is still a factor of 2 difference. On the other hand, in summer (Fig. 13c),
491 PERSIANN has many high rain rate events compared to the other estimates, and the seasonal
492 mean totals are correspondingly higher than the other estimates confirming what was already seen
493 in the time series results. One thing to note about the reanalysis estimates is that the rain amount

494 distributions tend to be narrower than the satellite and rain gauge estimates. This is most obvious
495 for ERAI (Fig. 13c) and becomes more severe for reanalyses with a coarser spatial resolution (not
496 shown), highlighting the fact that reanalyses only resolve a narrow band of rain rates. One notable
497 exception to this is MERRA2, which has equally high rain rates as PERSIANN. While this may
498 lead to positive results in midlatitude regions, it leads to estimated precipitation totals that are too
499 large (compared to the other estimates) by a factor of 2 over the maritime continent.

500 **5. Summary and Discussion**

501 A comparison of several global precipitation estimates and reanalyses was performed on a range
502 of temporal and spatial scales. Only data sets with daily or higher temporal resolution were con-
503 sidered. To minimize differences in the data sets due to resolution, all data sets with higher spatial
504 or temporal resolution than 1° , daily were interpolated to match the GPCP1DD resolution. We
505 found that while patterns of means and variance were largely consistent among data sets, the dif-
506 ferences in means and variances between the data sets were often as large as the analyzed means
507 and variances themselves.

508 Correlations among the precipitation estimates averaged over continental areas varied signifi-
509 cantly. GPCP1DD, TRMM and PERSICDR were very highly correlated. This was by construc-
510 tion on monthly and annual time scales, since all three data sets are bias corrected to monthly
511 satellite - rain gauge analyses (which use, and tend to be dominated by, the same GPCC analysis,
512 with the same undercatch-correction applied in all cases), but also held for daily averages. Corre-
513 lations of the satellite-only product, PERSIANN, with GPCP1DD were generally not significantly
514 different from zero on annual and daily timescales, but were on monthly time scales. Reanaly-
515 ses had high correlations with GPCP1DD on monthly time scales, but the results were mixed for
516 annual averages. Correlations between reanalyses and GPCP1DD were found to be larger than

517 0.8 over Europe and Australia, but results are mixed over North America. This is noteworthy,
518 because North America is one of the best observed regions in the world where the potential for
519 constraining reanalyses with observations is high. It is also interesting to note that correlations
520 with GAUGE+RT were comparable and larger than 0.79 for Europe, Australia and North Amer-
521 ica. This difference in the correlations with GPCP1DD versus GAUGERT in data dense regions
522 could reflect a difference in the data sources the different products assimilate.

523 The different time scale results for the correlations permit interesting speculation on some as-
524 pects of these precipitation estimates at different scales. The nature of the correlations (low at an-
525 nual and daily, higher at monthly time scales for time series averaged over large regions) could be
526 interpreted to suggest that large scale bias differences are large compared to interannual variability
527 and random errors are large at daily time scales, but that at intermediate time scales (monthly in
528 this case) the signal to noise ratio can be large enough to have high correlations. It would also
529 appear that monthly bias corrections increase daily correlations (e.g. PERSICDR and TRMM cor-
530 relations with GPCP1DD), possibly suggesting that the low correlations on daily time scales in
531 satellite-only products are a result of random errors and monthly bias.

532 Distributions of precipitation rates and amounts confirmed a known bias in satellite-only esti-
533 mates and showed that PERSIANN underestimated wintertime precipitation in midlatitudes, while
534 overestimating summertime precipitation in midlatitudes. Reanalyses tended to precipitate over
535 too narrow of a range of rain rates when compared to observational estimates, although some of
536 the reanalyses (JRA55 and MERRA2) estimate mean monthly totals in the same range as or even
537 above PERSIANN in the summer. The difference (at least for North America) is that the bulk of
538 the rain in the satellite-only estimate PERSIANN comes from high rain rates $> 2\text{mm h}^{-1}$, while
539 JRA55 overestimation occurred at rain rates around 0.8mm h^{-1} .

540 Average spread among data sets was computed for each grid point, and is defined as the average
541 of the standard deviation of anomalies from the seasonal cycle. Spread among data sets differed
542 between reanalyses and satellite estimates (Fig. 14). Spread among reanalyses was found to be
543 larger in the tropics and smaller in midlatitudes when compared to the spread among satellite esti-
544 mates. This is likely related to precipitation in midlatitudes being driven mainly by the large-scale
545 flow, while convective precipitation dominates in the tropics. Reanalyses do well in representing
546 mid-latitude large-scale circulation patterns and this results in higher consistency across reanaly-
547 ses in the mid-latitudes. In the tropics convective parameterizations were likely responsible for the
548 bulk of the precipitation in reanalyses; these parameterizations differed widely among reanalyses
549 and so did the results.

550 Systematic differences were found in the global precipitation estimates considered in this study.
551 Users of these estimates need to be aware of these biases and their use as a ground truth should
552 be limited to regimes, seasons, or regions the products have been shown to perform well for. For
553 example, PERSIANN and CMORPH, designed to represent the instantaneous variability in pre-
554 cipitation, performed well in the tropics, but overestimated summertime convective precipitation
555 and underestimated wintertime precipitation in midlatitudes. This suggests that the performance
556 of CMORPH and PERSIANN in midlatitude regions always needs to be assessed for the region
557 and season of interest prior to using these estimates. Reanalyses reflect the systematic errors of
558 the global circulation models used to provide the forecast background. There is a clear bias of the
559 reanalyses' annual and monthly means compared to the observational estimates. However, while
560 we showed here that large scale (continental to global) annual averages of precipitation estimates
561 differ in their interannual variability, variability estimated by reanalyses on monthly timescales
562 tends to be consistent with the observational estimates (as seen from the high correlations). This

563 suggests that studies interested mainly in the variability of precipitation may have a more reliable
564 foundation in using reanalyses than studies investigating the energy and water budgets.

565 In summary, any study using precipitation estimates based on observations or reanalyses should
566 take into account the uncertainty associated with the precipitation estimate. There is no one global
567 precipitation product that is better than all the others for all applications. The most suitable prod-
568 uct changes with intended application, location and season. Therefore, care needs to be taken
569 when choosing a product for a specific application, to ensure that the product has the capability
570 to yield useful results. Given the uncertainty inherent in any precipitation estimate it is an asset
571 to have several products based on different approaches available to compare and estimate that un-
572 certainty. In some ways precipitation estimates from satellite and reanalyses have the opposite
573 problem. Satellite estimates perform well in regions and seasons with convective precipitation,
574 while reanalyses are better at large scale precipitation in the northern midlatitudes. Precipitation
575 estimates that incorporate both satellite and ground-based measurements such as GPCP1DD, and
576 indirectly TRMM and PERSICDR, tend to lie in between the other estimates both in terms of
577 the distributions and the average rain rates. Incorporating ground radar in precipitation estimates
578 where available can be expected to have a positive impact on the accuracy of the estimates. In-
579 cluding data from diverse sources (multiple satellites and retrieval channels, rain gauge, radar)
580 appears to help with reducing errors and enhances reliability. Extending the rain gauge network
581 to data sparse regions, in particular over oceans, will likely have a large impact on constraining
582 at least global mean precipitation estimates. Unfortunately, this is impractical and costly. A more
583 practical approach may be to combine precipitation estimates from several different data sources
584 based on their respective strengths.

585 *Acknowledgments.* Gehne’s research is sponsored by the NWS Sandy Supplemental grant
586 NA14NWS4830003. Hamill’s research was funded by the Disaster Relief Appropriations Act
587 of 2013. Trenberth’s research is partially sponsored by DOE grant DE–SC0012711. NCAR is
588 sponsored by NSF. We would like to thank two anonymous reviewers for their comments and
589 insight. We would like to thank Reviewer 1 for suggesting the particular interpretation of the
590 correlation results. ERA-Interim data is provided courtesy of ECMWF and the Research Data
591 Archive at the National Center for Atmospheric Research. The CFSR dataset is provided from
592 the Climate Forecast System Reanalysis (CFSR) project carried out by the Environmental Model-
593 ing Center (EMC), National Centers for Environmental Prediction (NCEP). The (JRA55) dataset
594 is provided by the Japanese 55-year Reanalysis project carried out by the Japan Meteorological
595 Agency (JMA). MERRA was developed by the Global Modeling and Assimilation Office and
596 supported by the NASA Modeling, Analysis and Prediction Program. Source data files can be
597 acquired from the Goddard Earth Science Data Information Services Center (GES DISC).

598 **References**

- 599 Adam, J. C., and D. P. Lettenmaier, 2003: Adjustment of global gridded precipitation for system-
600 atic bias. *J. Geophys. Res.*, **108** (D9), doi:10.1029/2002JD002499.
- 601 Adler, R., and Coauthors, 2003: The version 2 global precipitation climatology project (GPCP)
602 monthly precipitation analysis (1979–present). *J. Hydrometeor.*, **4**, 1147–1167.
- 603 Adler, R. F., C. Kidd, G. Petty, M. Morrissey, H. M. Goodman, and F. Einaudi, 2001: Intercompar-
604 ison of global precipitation products: The third precipitation intercomparison project (PIP–3).
605 *Bull. Amer. Meteor. Soc.*, **82** (7), 1377–1396.

606 Ashouri, H., K.-L. Hsu, S. Sorooshian, D. K. Braithwaite, K. R. Knapp, L. D. Cecil, B. R. Nelson,
607 and O. P. Prat, 2015: PERSIANN-CDR: Daily precipitation climate data record from multisatel-
608 lite observations for hydrological and climate studies. *Bull. Amer. Meteor. Soc.*, **96** (1), 69–83,
609 doi:10.1175/BAMS-D-13-00068.1.

610 Becker, A., P. Finger, A. Meyer-Christoffer, B. Rudolf, K. Schamm, U. Schneider, and M. Ziese,
611 2013: A description of the global land-surface precipitation data products of the Global Precip-
612 itation Climatology Centre with sample applications including centennial (trend) analysis from
613 1901-present. *Earth Syst. Sci. Data*, **5** (1), 71–99, doi:10.5194/essd-5-71-2013.

614 Bell, T. L., A. Abdullah, R. L. Martin, and G. R. North, 1990: Sampling errors for satellite-
615 derived tropical rainfall: Monte carlo study using a space-time stochastic model. *J. Geophys.*
616 *Res.: Atmospheres*, **95** (D3), 2195–2205, doi:10.1029/JD095iD03p02195.

617 Bolvin, D., 2001: Global Precipitation at One-Degree Daily Resolution from Mul-
618 tiasatellite Observations, version 1.2. Accessed: 7 August 2014, NASA/GSFC,
619 <ftp://meso.gsfc.nasa.gov/pub/1dd-v1.2>.

620 Bosilovich, M. G., and Coauthors, 2015a: MERRA-2: Initial evaluation of the climate. Technical
621 Report Series on Global Modeling and Data Assimilation 43, National Aeronautics and Space
622 Administration.

623 Bosilovich, M. G., and Coauthors, 2015b: Modern-era retrospective analysis for research and
624 applications, version 2. Accessed: 9 February 2016, National Aeronautics and Space Adminis-
625 tration, <http://disc.sci.gsfc.nasa.gov/uui/search/\%22MERRA-2\%22>.

626 Braithwaite, D., 2000: PERSIANN: Precipitation Estimation from Remote Sensing Information
627 using Artificial Neural Networks. Accessed: 4 August 2014, Center for Hydrometeorology and

628 Remote Sensing, University of California, Irvine, <http://chrs.web.uci.edu/persiann/data.html>.

629 Brown, J. D., D.-J. Seo, and J. Du, 2012: Verification of precipitation forecasts from NCEPs short-
630 range ensemble forecast (SREF) system with reference to ensemble streamflow prediction using
631 lumped hydrologic models. *J. Hydrometeor.*, **13**, 808–836, doi:10.1175/JHM-D-11-036.1.

632 Chen, M., W. Shi, P. Xie, V. B. S. Silva, V. E. Kousky, R. W. Higgins, and J. E. Janowiak, 2008:
633 Assessing objective techniques for gauge-based analyses of global daily precipitation. *J. Geo-*
634 *phys. Res.*, **113**, D04 110, doi:10.1029/2007JD009132.

635 CMORPHv1.0, 2015: NOAA CPC Morphing Technique ("CMORPH"), Version 1.0, CRT. Ac-
636 cessed: 9 February 2016, NOAA Center for Weather and Climate Prediction, Climate Prediction
637 Center http://ftp.cpc.ncep.noaa.gov/precip/CMORPH_V1.0/CRT/.

638 Daly, C., R. P. Neilson, and D. L. Phillips, 1994: A statistical-topographic model for mapping
639 climatological precipitation over mountainous terrain. *J. Appl. Meteor.*, **33**, 140–158.

640 Dee, D. P., and Coauthors, 2011a: The ERA-Interim reanalysis: configuration and performance of
641 the data assimilation system. *Quart. J. Roy. Meteor. Soc.*, **137** (656), 553–597, doi:10.1002/qj.
642 828.

643 Dee, D. P., and Coauthors, 2011b: The ERA-Interim reanalysis. Accessed: 5 August 2014,
644 European Centre for Medium-Range Weather Forecasts, [http://www.ecmwf.int/en/research/](http://www.ecmwf.int/en/research/climate-reanalysis/era-interim)
645 [climate-reanalysis/era-interim](http://www.ecmwf.int/en/research/climate-reanalysis/era-interim).

646 Gutowski Jr., W. J., S. G. Decker, R. A. Donavon, Z. Pan, R. W. Arritt, and E. S. Takle, 2003: Tem-
647 poralspatial scales of observed and simulated precipitation in central U.S. climate. *J. Climate*,
648 **16**, 3841–3847, doi:10.1175/1520-0442(2003)016<3841:TSOOAS>2.0.CO;2.

649 Haerter, J. O., P. Berg, and S. Hagemann, 2010: Heavy rain intensity distributions on varying
650 time scales and at different temperatures. *J. Geophys. Res.*, **115** (D17), D17 102, doi:10.1029/
651 2009JD013384.

652 Hamill, T. M., 2012: Verification of TIGGE multimodel and ECMWF reforecast-calibrated proba-
653 bilistic precipitation forecasts over the contiguous united states. *Mon. Wea. Rev.*, **140** (7), 2232–
654 2252, doi:10.1175/MWR-D-11-00220.1.

655 Harris, I., P. Jones, T. Osborn, and D. Lister, 2014: Updated high-resolution grids of monthly
656 climatic observations - the CRU TS3.10 dataset. *Int. J. Climatol.*, **34** (3), 623–642, doi:10.1002/
657 joc.3711.

658 Hsu, K.-l., X. Gao, S. Sorooshian, and H. V. Gupta, 1997: Precipitation estimation from remotely
659 sensed information using artificial neural networks. *J. Appl. Meteor.*, **36**, 1176–1190.

660 Huffman, G., E. Stocker, D. Bolvin, E. Nelkin, and R. Adler, 2012: TRMM Ver-
661 sion 7 3B42 and 3B43 Data Sets. Accessed: 5 January 2014, NASA/GSFC,
662 [http://mirador.gsfc.nasa.gov/cgi-bin/mirador/presentNavigation.pl?tree=project&project=](http://mirador.gsfc.nasa.gov/cgi-bin/mirador/presentNavigation.pl?tree=project&project=TRMM&dataGroup=Gridded&CGISESSID=5d12e2ffa38ca2aac6262202a79d882a)
663 [TRMM&dataGroup=Gridded&CGISESSID=5d12e2ffa38ca2aac6262202a79d882a](http://mirador.gsfc.nasa.gov/cgi-bin/mirador/presentNavigation.pl?tree=project&project=TRMM&dataGroup=Gridded&CGISESSID=5d12e2ffa38ca2aac6262202a79d882a).

664 Huffman, G. J., R. F. Adler, M. M. Morrissey, D. T. Bolvin, S. Curtis, R. Joyce, B. McGavock,
665 and J. Susskind, 2000: Global precipitation at one-degree daily resolution from multisatellite
666 observations. *J. Hydrometeor.*, **2**, 36–50.

667 Huffman, G. J., and Coauthors, 1997: The Global Precipitation Climatology Project (GPCP) com-
668 bined precipitation dataset. *Bull. Amer. Meteor. Soc.*, **78**, 5–20.

669 Huffman, G. J., and Coauthors, 2007: The TRMM multi satellite precipitation analysis (TMPA):
670 Quasi-global, multiyear, combined-sensor precipitation estimates at fine scales. *J. Hydrometeor.*,
671 **8**, 38–55, doi:10.1175/JHM560.1.

672 Janowiak, J. E., P. Bauer, W. Wang, P. A. Arkin, and J. Gottschalck, 2010: An evaluation of
673 precipitation forecasts from operational models and reanalyses including precipitation variations
674 associated with MJO activity. *Mon. Wea. Rev.*, **138**, 4542–4560, doi:10.1175/2010MWR3436.1.

675 Joyce, B., and J. Janowiak, 2005: NOAA CPC Morphing Technique (“CMORPH”). Accessed:
676 7 January 2014, NOAA Climate Prediction Center, [http://www.cpc.ncep.noaa.gov/products/
677 janowiak/cmorph_description.html](http://www.cpc.ncep.noaa.gov/products/janowiak/cmorph_description.html).

678 Joyce, R. J., J. E. Janowiak, P. A. Arkin, and P. Xie, 2004: CMORPH: A method that produces
679 global precipitation estimates from passive microwave and infrared data at high spatial and
680 temporal resolution. *J. Hydrometeor.*, **5**, 487–503.

681 Kennedy, A. D., X. Dong, B. Xi, S. Xie, Y. Zhang, and J. Chen, 2011: A comparison of MERRA
682 and NARR reanalyses with the DOE ARM SGP data. *J. Climate*, **24** (17), 4541–4557, doi:
683 10.1175/2011JCLI3978.1.

684 Kidd, C., P. Bauer, J. Turk, G. J. Huffman, R. Joyce, K. L. Hsu, and D. Braithwaite, 2012: Inter-
685 comparison of high-resolution precipitation products over northwest Europe. *J. Hydrometeor.*,
686 **13** (1), 67–83, doi:10.1175/JHM-D-11-042.1.

687 Kidd, C., and G. Huffman, 2011: Global precipitation measurement. *Meteorol. Appl.*, **18** (3), 334–
688 353, doi:10.1002/met.284.

- 689 Kobayashi, S., and Coauthors, 2015a: The JRA-55 reanalysis. Accessed: June 2015, Research
690 Data Archive at the National Center for Atmospheric Research, [http://rda.ucar.edu/datasets/
691 ds628.0/](http://rda.ucar.edu/datasets/ds628.0/).
- 692 Kobayashi, S., and Coauthors, 2015b: The JRA-55 reanalysis: General specifications and basic
693 characteristics. *J. Meteor. Soc. Japan*, **93** (1), 5–48, doi:10.2151/jmsj.2015-001.
- 694 Lien, G.-Y., T. Miyoshi, and E. Kalnay, 2015: Assimilation of TRMM multisatellite precipitation
695 analysis with a low-resolution NCEP global forecasting system. *Mon. Wea. Rev.*, **144**, 643–661,
696 doi:10.1175/MWR-D-15-0149.1.
- 697 Lin, Y., and K. E. Mitchell, 2005: The NCEP stage II/IV hourly precipitation analyses: Devel-
698 opment and applications, pre-prints, 19th Conf. on Hydrology, San Diego, CA, Amer. Meteor.
699 Soc., 1.2. Available online at <https://ams.confex.com/ams/pdfpapers/83847.pdf>.
- 700 Lindvall, J., G. Svensson, and C. Hannay, 2013: Evaluation of near-surface parameters in the two
701 versions of the atmospheric model in CESM1 using flux station observations. *J. Climate*, **26**,
702 26–44, doi:10.1175/JCLI-D-12-00020.1.
- 703 Liu, Q., and Coauthors, 2011: The contributions of precipitation and soil moisture observations
704 to the skill of soil moisture estimates in a land data assimilation system. *J. Hydrometeor.*, **12**,
705 750–765, doi:10.1175/JHM-D-10-05000.1.
- 706 McLaughlin, D., Y. Zhou, D. Entekhabi, and V. Chatdarong, 2006: Computational issues for
707 large-scale land surface data assimilation problems. *J. Hydrometeor.*, **7** (3), 494–510, doi:10.
708 1175/JHM493.1.

- 709 Meng, J., R. Yang, H. Wei, M. Ek, G. Gayno, P. Xie, and K. Mitchell, 2012: The land surface
710 analysis in the NCEP climate forecast system reanalysis. *J. Hydrometeor.*, **13** (5), 1621–1630,
711 doi:10.1175/JHM-D-11-090.1.
- 712 Mesinger, F., and Coauthors, 2006: North American Regional Reanalysis. *Bull. Amer. Meteor.*
713 *Soc.*, **87** (3), 343–360, doi:10.1175/BAMS-87-3-343.
- 714 Peterson, T. C., and Coauthors, 1998: Homogeneity adjustments of in situ atmospheric climate
715 data: a review. *Int. J. Climatol.*, **18** (13), 1493–1517.
- 716 Prat, O. P., and B. R. Nelson, 2015: Evaluation of precipitation estimates over CONUS derived
717 from satellite, radar, and rain gauge data sets at daily to annual scales (20022012). *Hydrol. Earth*
718 *Syst. Sci.*, **19**, 2037–2056, doi:10.5194/hess-19-2037-2015,2015.
- 719 Rienecker, M., and Coauthors, 2011a: MERRA: NASA’s modern-era retrospective analysis for
720 research and applications. *J. Climate*, **24**, 3624–3648, doi:10.1175/JCLI-D-11-00015.1.
- 721 Rienecker, M., and Coauthors, 2011b: MERRA: NASA’s modern-era retrospective analysis for
722 research and applications. Accessed: August 2014, National Aeronautics and Space Adminis-
723 tration, <http://disc.sci.gsfc.nasa.gov/uui/search/%22MERRA%22>.
- 724 Rodell, M., and Coauthors, 2015: The observed state of the water cycle in the early twenty-first
725 century. *J. Climate*, **28** (21), 8289–8318, doi:10.1175/JCLI-D-14-00555.1.
- 726 Ruane, A. C., 2010a: NARR’s atmospheric water cycle components. part i: 20-year mean and
727 annual interactions. *J. Hydrometeor.*, **11** (6), 1205–1219, doi:10.175/2010JHM1193.1.
- 728 Ruane, A. C., 2010b: NARR’s atmospheric water cycle components. part ii: Summertime mean
729 and diurnal interactions. *J. Hydrometeor.*, **11** (6), 1220–1233, doi:10.1175/2010JHM1279.1.

730 Saha, S., and Coauthors, 2010a: The NCEP climate forecast system reanalysis. *Bull. Amer. Meteor.*
731 *Soc.*, **91** (8), 1015–1057, doi:10.1175/2010BAMS3001.1.

732 Saha, S., and Coauthors, 2010b: The NCEP climate forecast system reanalysis. Accessed: August
733 2014, Research Data Archive at the National Center for Atmospheric Research, [http://rda.ucar.](http://rda.ucar.edu/datasets/ds093.0/)
734 [edu/datasets/ds093.0/](http://rda.ucar.edu/datasets/ds093.0/).

735 Sapiano, M. R. P., and P. A. Arkin, 2009: An intercomparison and validation of high-resolution
736 satellite precipitation estimates with 3-hourly gauge data. *J. Hydrometeor.*, **10**, 149–166, doi:
737 10.1175/2008JHM1052.1.

738 Schlosser, C. A., and P. R. Houser, 2007: Assessing a satellite-era perspective of the global water
739 cycle. *J. Climate*, **20** (7), 1316–1338, doi:10.1175/JCLI4057.1.

740 Smith, E. A., J. E. Lamm, and R. Adler, 1998: Results of WetNet PIP-2 project. *J. Atmos. Sci.*, **55**,
741 1483–1536.

742 Sohn, B. J., H.-J. Han, and E.-K. Seo, 2010: Validation of satellite-based high-resolution rainfall
743 products over the korean peninsula using data from a dense rain gauge network. *J. Appl. Meteor.*
744 *Climatol.*, **49** (4), 701–714, doi:10.1175/2009JAMC2266.1.

745 Sorooshian, S., K. Hsu, D. Braithwaite, H. Ashouri, and N. C. Program, 2014: NOAA Climate
746 Data Record (CDR) of Precipitation Estimation from Remotely Sensed Information using Ar-
747 tificial Neural Networks (PERSIANN-CDR), Version 1 Revision 1. Accessed: 28 July 2015,
748 NOAA National Climatic Data Center, <ftp://data.ncdc.noaa.gov/cdr/persiann/files/>.

749 Sorooshian, S., K.-L. Hsu, X. Gao, H. V. Gupta, B. Imam, and D. Braithwaite, 2000: Evaluation
750 of PERSIANN system satellite-based estimates of tropical rainfall. *Bull. Amer. Meteor. Soc.*,
751 **81**, 2035–2046.

- 752 Stephens, G. L., and Coauthors, 2010: Dreary state of precipitation in global models. *J. Geophys.*
753 *Res.*, **115 (D24)**, doi:10.1029/2010JD014532, d24211.
- 754 Trenberth, K. E., A. Dai, R. M. Rasmussen, and D. B. Parsons, 2003: The changing character of
755 precipitation. *Bull. Amer. Meteor. Soc.*, **84**, 1205–1217, doi:10.1175/2008BAMS2634.1.
- 756 Trenberth, K. E., A. Dai, G. van der Schrier, P. D. Jones, J. Barichivich, K. R. Briffa, and
757 J. Sheffield, 2014: Global warming and changes in drought. *Nature Climate Change*, **4**, 17–
758 22, doi:10.1038/NCLIMATE2067.
- 759 Trenberth, K. E., and J. T. Fasullo, 2013: Regional energy and water cycles: Transports from
760 ocean to land. *J. Climate*, **26**, 7837–7851, doi:10.1175/JCLI-D-13-00008.1.
- 761 Trenberth, K. E., J. T. Fasullo, and J. Kiehl, 2009: Earth’s global energy budget. *Bull. Amer.*
762 *Meteor. Soc.*, **90**, 311–323, doi:10.1175/2008BAMS2634.1.
- 763 Trenberth, K. E., J. T. Fasullo, and J. Mackaro, 2011: Atmospheric Moisture Transports from
764 Ocean to Land and Global Energy Flows in Reanalyses. *J. Climate*, **24 (18)**, 4907–4924.
- 765 Trenberth, K. E., and D. J. Shea, 2005: Relationships between precipitation and surface tempera-
766 ture. *Geophys. Res. Lett.*, **32 (14)**, L14 703, doi:10.1029/2005GL022760.
- 767 Trenberth, K. E., L. Smith, T. Qian, A. Dai, and J. Fasullo, 2007: Estimates of the global water
768 budget and its annual cycle using observational and model data. *J. Hydrometeor.*, **8 (4)**, 758–769,
769 doi:10.1175/JHM600.1.
- 770 Wilcox, E. M., and L. J. Donner, 2007: The frequency of extreme rain events in satellite rain-rate
771 estimates and an atmospheric general circulation model. *J. Climate*, **20**, 53–69, doi:10.1175/
772 JCLI3987.1.

773 Wolff, D. B., and B. L. Fisher, 2008: Comparisons of instantaneous TRMM ground validation and
774 satellite rain-rate estimates at different spatial scales. *J. Appl. Meteor. Climatol.*, **47**, 2215–2237,
775 doi:10.1175/2008JAMC1875.1.

776 Xie, P., 2009: CPC Unified Gauge-Based Analysis of Global Daily Precipitation. Accessed: 5
777 August 2014, NOAA Climate Prediction Center, http://ftp.cpc.ncep.noaa.gov/precip/CPC_UNI_
778 [PRCP](http://ftp.cpc.ncep.noaa.gov/precip/CPC_UNI_PRCP).

779 Xie, P., and P. A. Arkin, 1997: Global precipitation: a 17-year monthly analysis based on gauge
780 observations, satellite estimates, and numerical model outputs. *Bull. Amer. Meteor. Soc.*, **78**,
781 2539–2558.

782 Xie, P., M. Chen, S. Yang, A. Yatagai, T. Hayasaka, Y. Fukushima, and C. Liu, 2007: A gauge-
783 based analysis of daily precipitation over East Asia. *J. Hydrometeor.*, **8**, 607–627, doi:10.1175/
784 JHM583.1.

785 Yatagai, A., K. Kamiguchi, O. Arakawa, A. Hamada, N. Yasutomi, and A. Kitoh, 2012:
786 APHRODITE: Constructing a long-term daily gridded precipitation dataset for Asia based
787 on a dense network of rain gauges. *Bull. Amer. Meteor. Soc.*, **93**, 1401–1415, doi:10.1175/
788 BAMS-D-11-00122.1.

LIST OF TABLES

789		
790	Table 1.	List of precipitation estimate data sets. Sources are geostationary infrared (Geo-IR), microwave (MW), gauges, or reanalyses. Only the main data set reference is given for each data set. Additional references and references with links to the actual data sets are included with the description of the data sets in section 2. 38
791		
792		
793		
794		
795	Table 2.	Description of the metrics used in the analysis. $P(x, y, d, m, yr)$ is precipitation at longitude x , latitude y , day d , month m , and year yr . N_m is the total number of days in month m , $m = 1, \dots, 12$. N_A is the number of grid points in region A with $(x_i, y_j) \in A$. w_j are the weights that account for changing area of the grid box with latitude. P_1, \dots, P_{N_d} are the different data sets, with N_d the total number of data sets. M is the mean of all the precipitation data sets. 39
796		
797		
798		
799		
800		
801	Table 3.	Description of continental regions used in the analysis. Only points over land inside the domains are used. Also shown are the amplitude (mm d^{-1}) of the area averaged mean annual cycle for 2001-2012 and the phase (the day of the year the maximum occurs). The annual cycle is defined as the first 4 harmonics of the mean daily annual cycle. These are given for all data sets in the order (TRMM, GPCP1DD, CMORPHCRT, PERSIANN, PERSICDR, GAUGE+RT, JRA55, MERRA2, CFSR, ERAI). The minimum and maximum are highlighted in bold. 40
802		
803		
804		
805		
806		
807		
808		
809	Table 4.	Correlations between GPCP1DD and all other data sets for annual, monthly and daily mean time series. Correlations are computed for common time period 2001-2012 (2001-2010 for CFSR) with the annual cycle removed. The annual cycle is defined as the first 4 harmonics of the mean daily seasonal cycle. Correlations significant at the 90% level are bold. 41
810		
811		
812		
813		

814 TABLE 1. List of precipitation estimate data sets. Sources are geostationary infrared (Geo-IR), microwave
815 (MW), gauges, or reanalyses. Only the main data set reference is given for each data set. Additional references
816 and references with links to the actual data sets are included with the description of the data sets in section 2.

Name	Source	Temporal resolution	Spatial resolution	Reference
TRMM (TRMM3B42)	Geo-IR; MW from SSM/I,TMI, AMSU, AMSR; gauges	1998 - 2012, 3 hourly	49°S - 49°N 0.25°	Huffman et al. (2007)
CMORPH (V0.x)	Geo-IR; MW from SSM/I,TMI, AMSU, AMSR;	2003 - 2013, 3 hourly	59°S - 59°N 0.25°	Joyce et al. (2004)
CMORPHCRT (V1.0)	Geo-IR; MW from SSM/I,TMI, AMSU, AMSR;	1998 - 2013, 3 hourly	59°S - 59°N 0.25°	Joyce et al. (2004)
PERSIANN	Geo-IR; MW from TMI	2001 - 2013, 3hourly	59°S - 59°N 0.25°	Hsu et al. (1997) Sorooshian et al. (2000)
PERSICDR (V1.R1)	Geo-IR; MW from TMI (for training) SSM/I; IR; gauges	1983 - 2013, daily	60°S - 60°N 0.25°	Ashouri et al. (2015)
GPCP1DD	Geo-IR; AVHRR low-earth-orbit IR, SSM/I; gauges; TOVS (poleward of 40S-40N)	1997 - 2013, daily	global, 1°	Huffman et al. (2000)
GAUGE	gauges	1979 - 2005, daily	global land, 0.5°	Xie et al. (2007); Chen et al. (2008)
GAUGERT	gauges	2006 - 2013, daily	global land, 0.5°	Xie et al. (2007); Chen et al. (2008)
JRA55	Reanalysis	1979 - 2013, 3hourly	global, gaussian 0.5625°	Kobayashi et al. (2015b)
MERRA	Reanalysis	1979 - 2013, hourly	global, 0.5° x 2/3°	Rienecker et al. (2011a)
MERRA2	Reanalysis	1980 - 2015, hourly	global, 0.5° x 0.625°	Bosilovich et al. (2015a)
CFSR	Reanalysis	1979 - 2010, 6hourly	global, 0.5°	Saha et al. (2010a)
ERA-Interim	Reanalysis	1979 - 2013, 3hourly	global, 0.75°	Dee et al. (2011a)

817 TABLE 2. Description of the metrics used in the analysis. $P(x, y, d, m, yr)$ is precipitation at longitude x ,
818 latitude y , day d , month m , and year yr . N_m is the total number of days in month m , $m = 1, \dots, 12$. N_A is the
819 number of grid points in region A with $(x_i, y_j) \in A$. w_j are the weights that account for changing area of the grid
820 box with latitude. P_1, \dots, P_{N_d} are the different data sets, with N_d the total number of data sets. M is the mean of
821 all the precipitation data sets.

Metric	
Monthly mean	$\bar{P}(x, y, m) = \frac{1}{N_m} \sum_{yr=1}^N \sum_{k=1}^{N_{my}} P(x, y, d_k, m, yr)$
Monthly variance	$\sigma^2(x, y, m) = \frac{1}{N_m} \sum_{yr=1}^N \sum_{k=1}^{N_{my}} (P(x, y, d_k, m, yr) - \bar{P}(x, y, m))^2$
Difference	$D(x, y, m) = \bar{P}(x, y, m) - \bar{Q}(x, y, m)$
Percentage difference	$D(x, y, m) = \frac{\bar{P}(x, y, m) - \bar{Q}(x, y, m)}{\bar{P}(x, y, m)} * 100$
Spatial average	$P_A(d, m, yr) = \frac{1}{N_A} \sum_{i=1}^{N_{xA}} \sum_{j=1}^{N_{yA}} w_j P(x_i, y_j, d, m, yr)$
Spread among data sets	$\sigma_P(x, y) = \frac{1}{N_t} \sum_{k=1}^{N_t} \sqrt{\frac{1}{N_d} \sum_{d=1}^{N_d} (P_d(x, y, t_k) - M(x, y, t_k))^2}$

822 TABLE 3. Description of continental regions used in the analysis. Only points over land inside the domains
823 are used. Also shown are the amplitude (mm d^{-1}) of the area averaged mean annual cycle for 2001-2012 and
824 the phase (the day of the year the maximum occurs). The annual cycle is defined as the first 4 harmonics of
825 the mean daily annual cycle. These are given for all data sets in the order (TRMM, GPCP1DD, CMORPHCRT,
826 PERSIANN, PERSICDR, GAUGE+RT, JRA55, MERRA2, CFSR, ERAI). The minimum and maximum are
827 highlighted in bold.

Region	lon-lat	Amplitude	Phase
North America	165°W - 50°W	(1.47, 1.19, 1.22, 1.22, 1.19,	(270, 273, 276 , 256, 271,
	15°N - 49°N	1.38, 1.5 , 1.33, 1.37, 1.16)	253 , 266, 264, 272, 272)
South America	90°W - 30°W	(1.26, 1.25, 1.08, 1.57, 1.25,	(75, 73, 73, 304 , 71,
	49°S - 15°N	3.35 , 1.2, 1.4, 1.51, 1.01)	59, 328, 91 , 84, 340)
Europe	15°W - 50°E	(1.62, 1.51, 1.12, 0.45 , 1.47,	(321, 336, 310, 298 , 339,
	30°N - 49°N	0.77, 1.21, 1.27, 1.69 , 1.02)	321, 328, 331, 344 , 330)
Africa	20°W - 50°E	(0.67, 0.57, 0.56 , 0.88 , 0.6,	(92, 87 , 96, 93, 88,
	35°S - 30°N	0.79, 0.77, 0.88 , 0.61, 0.74)	228 , 87 , 93, 92, 89)
Asia	50°E - 150°E	(4.09, 3.78, 3.54, 3.8, 3.87,	(204, 203, 206, 196 , 202,
	5°N - 49°N	2.99 , 5.12 , 4.99, 4.39, 3.38)	202, 204, 207 , 203, 207)
Maritime Continent	90°E - 165°E	(3.19, 3 , 3.13, 4.56, 3.03,	(364, 4, 365, 18, 5,
	10°S - 5°N	4.39, 4.43, 5.15 , 3.64, 3.21)	354 , 363, 366, 19 , 2)
Australia	110°E - 155°E	(3.05, 2.84, 2.89, 4.02 , 2.88,	(42, 43, 41, 34 , 43,
	49°S - 10°S	3.06, 3.52, 3.46, 2.41, 2.04)	41, 40, 42, 43, 46)

828 TABLE 4. Correlations between GPCP1DD and all other data sets for annual, monthly and daily mean time
829 series. Correlations are computed for common time period 2001-2012 (2001-2010 for CFSR) with the annual
830 cycle removed. The annual cycle is defined as the first 4 harmonics of the mean daily seasonal cycle. Correlations
831 significant at the 90% level are bold.

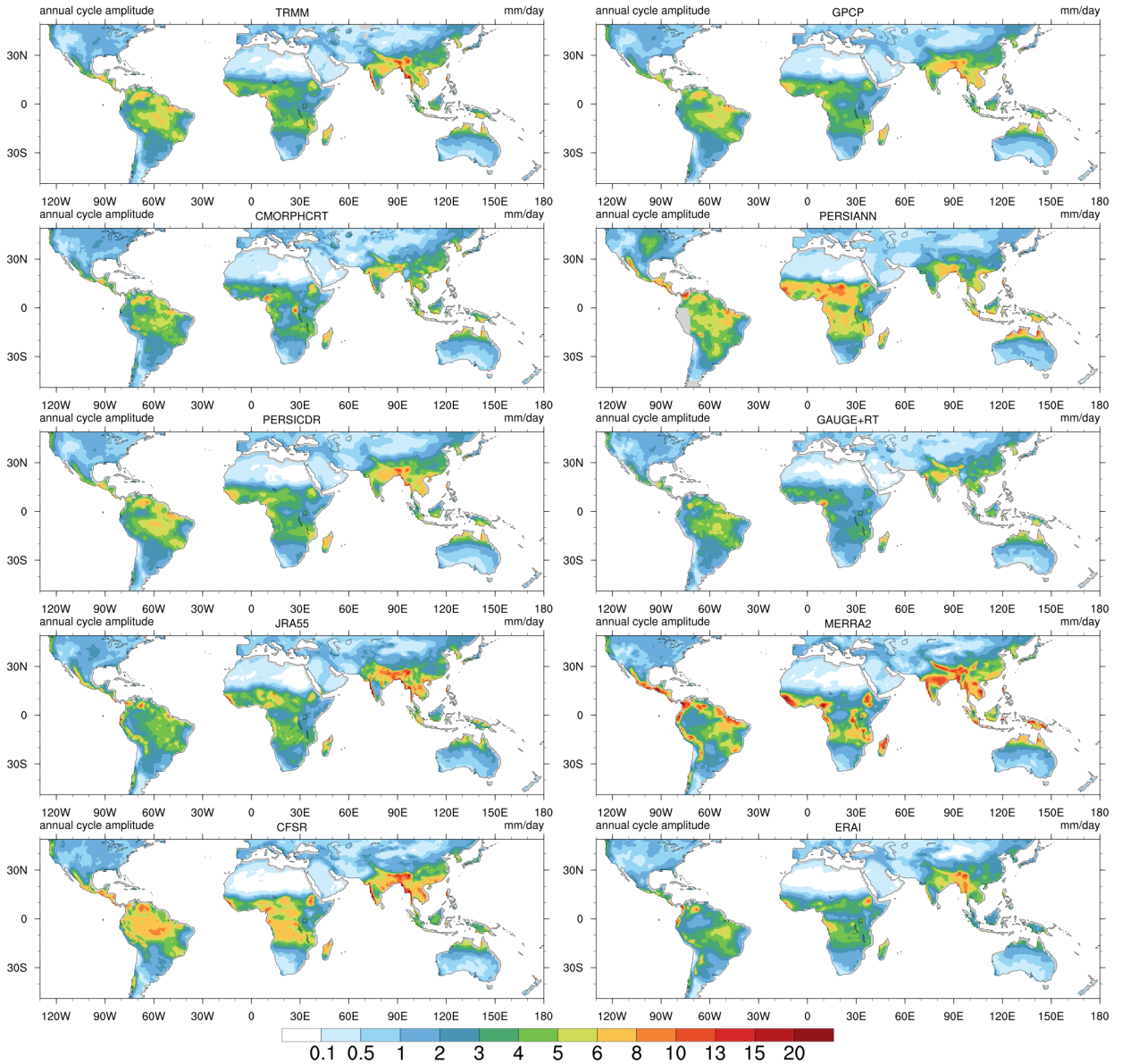
	GAUGE+RT	TRMM	CMORPHCRT	PERSIANN	PERSICDR	JRA55	MERRA2	MERRA	CFSR	ERA-Interim
Annual										
North America	0.82	0.97	0.49	0.17	0.99	0.46	0.81	0.83	0.56	0.56
South America	0.25	0.99	0.31	-0.19	1.00	0.66	0.49	0.57	0.44	0.71
Europe	0.81	0.97	0.34	-0.01	0.99	0.92	0.85	0.95	0.79	0.88
Africa	0.56	0.98	0.26	0.69	1.00	0.60	0.22	0.74	0.29	0.55
Asia	0.77	0.95	0.76	0.06	0.99	0.75	0.75	0.46	0.48	0.61
maritime continent	0.94	0.99	0.98	0.14	1.00	0.94	0.14	0.80	0.97	0.91
Australia	0.98	1.00	0.98	0.85	1.00	0.95	0.97	0.95	0.95	0.98
Monthly										
North America	0.55	0.92	0.36	0.38	0.98	0.84	0.52	0.87	0.84	0.83
South America	0.25	0.96	0.26	0.20	0.98	0.75	0.29	0.66	0.50	0.70
Europe	0.71	0.95	0.47	0.27	0.99	0.95	0.60	0.95	0.95	0.94
Africa	0.73	0.98	0.39	0.44	1.00	0.67	0.58	0.67	0.67	0.67
Asia	0.88	0.98	0.83	0.29	1.00	0.90	0.86	0.82	0.82	0.89
maritime continent	0.92	0.98	0.94	0.52	1.00	0.87	0.61	0.86	0.92	0.84
Australia	0.99	1.00	0.97	0.78	1.00	0.96	0.97	0.96	0.96	0.98
Daily										
North America	0.28	0.75	0.62	0.03	0.91	0.71	0.57	0.60	0.68	0.65
South America	0.23	0.83	0.70	-0.01	0.91	0.71	0.57	0.65	0.63	0.64
Europe	0.48	0.78	0.60	0.02	0.90	0.67	0.55	0.64	0.66	0.64
Africa	0.31	0.87	0.71	-0.02	0.96	0.72	0.63	0.61	0.52	0.63
Asia	0.34	0.86	0.84	-0.06	0.96	0.81	0.79	0.69	0.77	0.75
maritime continent	0.40	0.92	0.91	-0.03	0.99	0.81	0.80	0.76	0.81	0.76
Australia	0.65	0.90	0.89	-0.00	0.97	0.85	0.86	0.80	0.82	0.82

LIST OF FIGURES

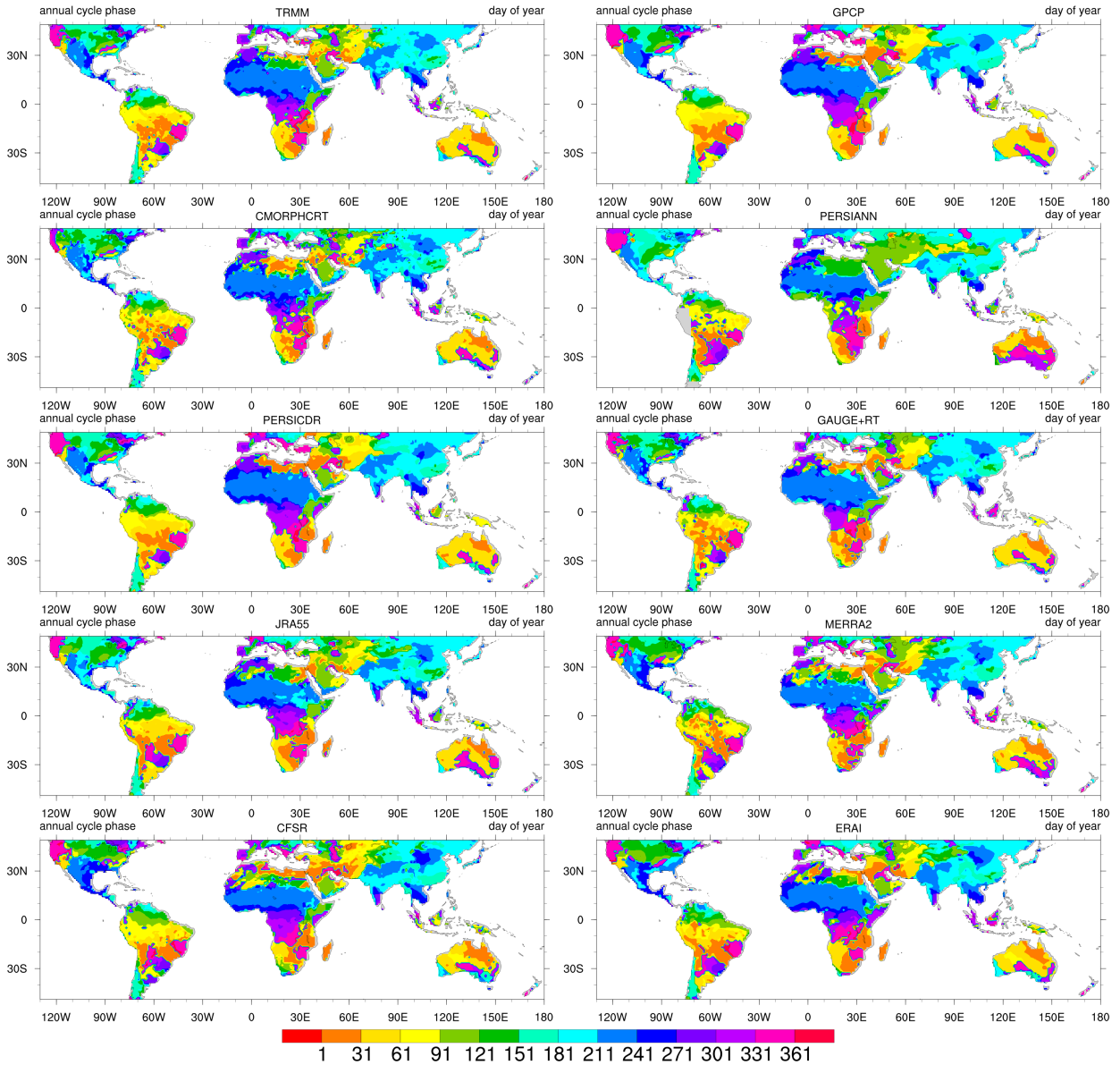
832		
833	Fig. 1.	Annual cycle amplitude in mm d^{-1} for the 10 datasets for 2001 – 2012. The annual cycle is
834		computed as the first 4 harmonics of the mean daily seasonal cycle. The amplitude is half of
835		the difference between the minimum and maximum of the annual cycle. 44
836	Fig. 2.	Annual cycle phase in day of year for the 10 datasets for 2001 – 2012. The annual cycle is
837		computed as the first 4 harmonics of the mean daily seasonal cycle. The phase is the day of
838		the year the maximum of the annual cycle is achieved. 45
839	Fig. 3.	Mean annual cycle for the 10 datasets for 2001 – 2012 averaged over the continental regions.
840		The annual cycle is computed as the first 4 harmonics of the mean daily seasonal cycle at
841		each grid point and then averaged over the continental regions. 46
842	Fig. 4.	Monthly long term means of precipitation for July. a) mean for GPCP1DD. b)-f) the differ-
843		ence between GPCP1DD mean and the respective data set mean for the period is indicated in
844		shading, contours show the mean monthly precipitation for the respective data set. Contour
845		levels go from 0 to 0.4 by 0.1mm h^{-1} 47
846	Fig. 5.	Same as in Fig. 4, but for January. 48
847	Fig. 6.	Monthly long term means of precipitation and percentage difference for July. a) mean for
848		GPCP1DD. b)-f) the percentage difference between GPCP1DD mean and the respective data
849		set mean for the period is indicated in shading, contours show the mean monthly precipita-
850		tion for the respective data set. Contour levels as in Fig. 4. 49
851	Fig. 7.	Monthly mean variance of precipitation for July. a) mean variance for GPCP1DD. b)-f) the
852		difference between the GPCP1DD mean variance and the respective data set mean variance
853		for the period is indicated in shading, contours show the mean monthly precipitation variance
854		for the respective data set. Contour levels are (0.001, 0.002, 0.005, 0.01, 0.1, 1, 2, 10). 50
855	Fig. 8.	Same as in Fig. 7, but for January. 51
856	Fig. 9.	Time series of rain rates averaged over global land area between 49°N and 49°S for a) annual
857		means, and b) monthly means. 52
858	Fig. 10.	Time series of rain rates averaged over North America land area between 15°N – 49°N for a)
859		annual means, b) monthly means, and c) weekly means. 53
860	Fig. 11.	Percentage distribution of precipitation rate over land area for North America (15°N - 49°N ,
861		195°E - 310°E). Panels a)-d) show the climatological distribution for all seasons for 2001 -
862		2012. Precipitation rates are binned with logarithmic bin sizes to account for more frequent
863		rain events at low rain rates. The x axis is plotted on a log-scale and the y axis on a linear
864		scale to compare the bulk of the distribution, not the tails. The black line shows the size of
865		the bin at each precipitation rate. Distributions are computed for each month and grid point
866		separately and then averaged over area and season. 54
867	Fig. 12.	Percentage distribution of precipitation rate over land area for North America (15°N - 49°N ,
868		195°E - 310°E). As in Fig. 11, except that the x axis is plotted on a linear scale and the y
869		axis on a log scale to facilitate comparison of the tails of the distributions. 55
870	Fig. 13.	Distribution of precipitation amount by precipitation rate over land area for North America
871		(15°N - 49°N , the same area as is used in Fig. 10). Panels a)-d) show the precipitation

872 amount distribution for all seasons for 2001 - 2012. The average is computed over the
873 years 2001 - 2012. Insets show average monthly totals during each season for the different
874 estimates. 56

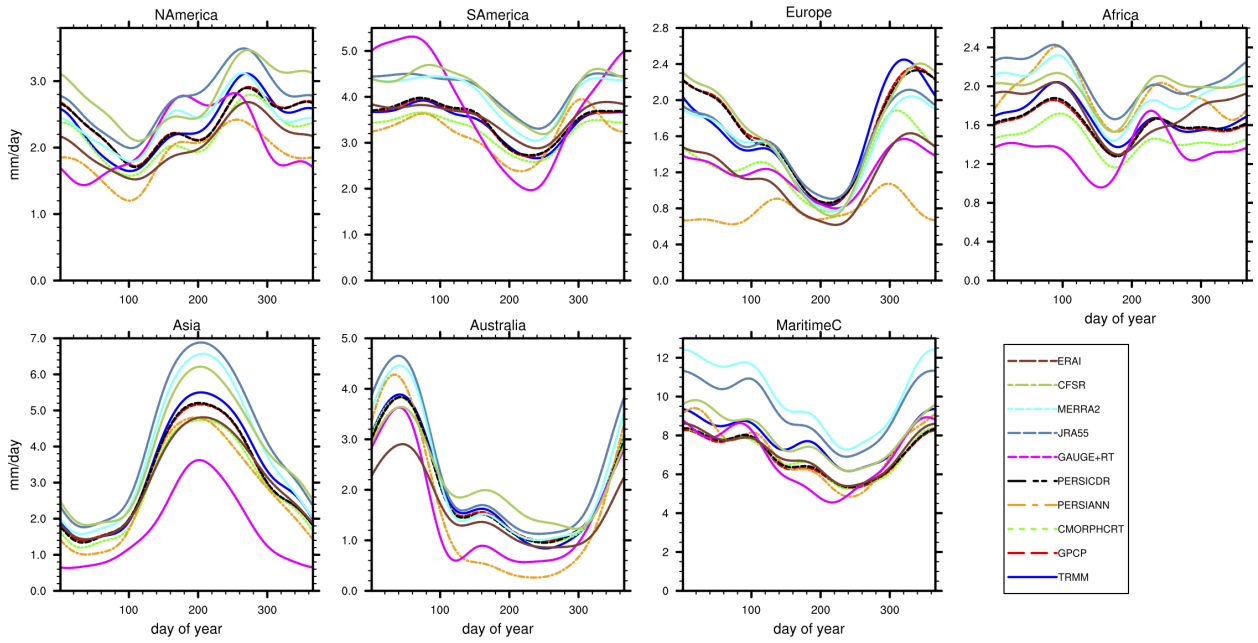
875 **Fig. 14.** Spread among precipitation estimates (computed as the mean standard deviation among data
876 sets) for 2001-2010. Top panel: spread among precipitation data sets (including reanalyses).
877 Bottom panel: difference in spread among observational precipitation data sets and spread
878 among reanalyses. The mean seasonal cycle is removed from daily data prior to computing
879 the spread. 57



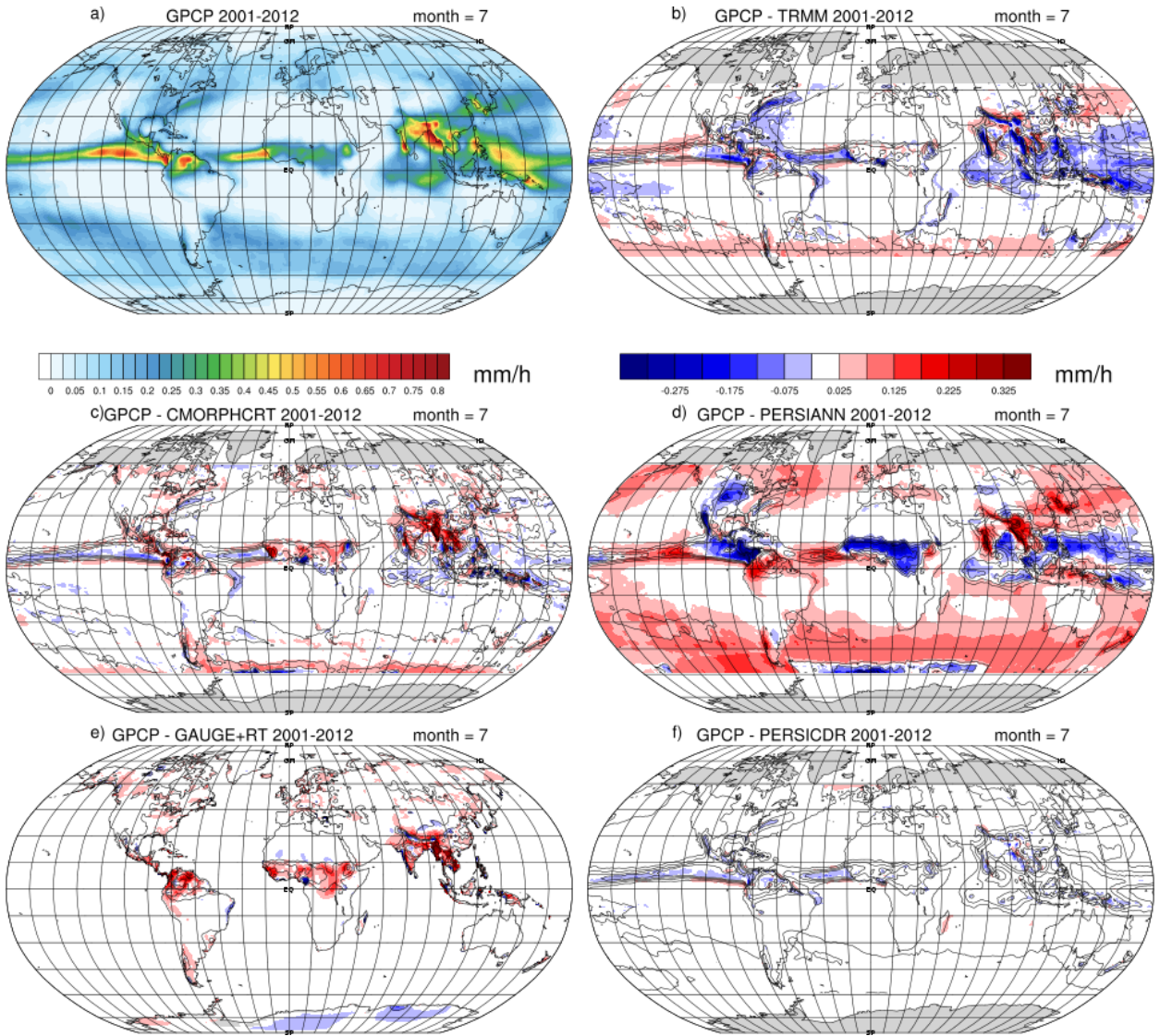
880 FIG. 1. Annual cycle amplitude in mm d^{-1} for the 10 datasets for 2001 – 2012. The annual cycle is computed
 881 as the first 4 harmonics of the mean daily seasonal cycle. The amplitude is half of the difference between the
 882 minimum and maximum of the annual cycle.



883 FIG. 2. Annual cycle phase in day of year for the 10 datasets for 2001 – 2012. The annual cycle is computed
 884 as the first 4 harmonics of the mean daily seasonal cycle. The phase is the day of the year the maximum of the
 885 annual cycle is achieved.



886 FIG. 3. Mean annual cycle for the 10 datasets for 2001 – 2012 averaged over the continental regions. The
 887 annual cycle is computed as the first 4 harmonics of the mean daily seasonal cycle at each grid point and then
 888 averaged over the continental regions.



889 FIG. 4. Monthly long term means of precipitation for July. a) mean for GPCP1DD. b)-f) the difference
 890 between GPCP1DD mean and the respective data set mean for the period is indicated in shading, contours show
 891 the mean monthly precipitation for the respective data set. Contour levels go from 0 to 0.4 by 0.1mm h⁻¹.

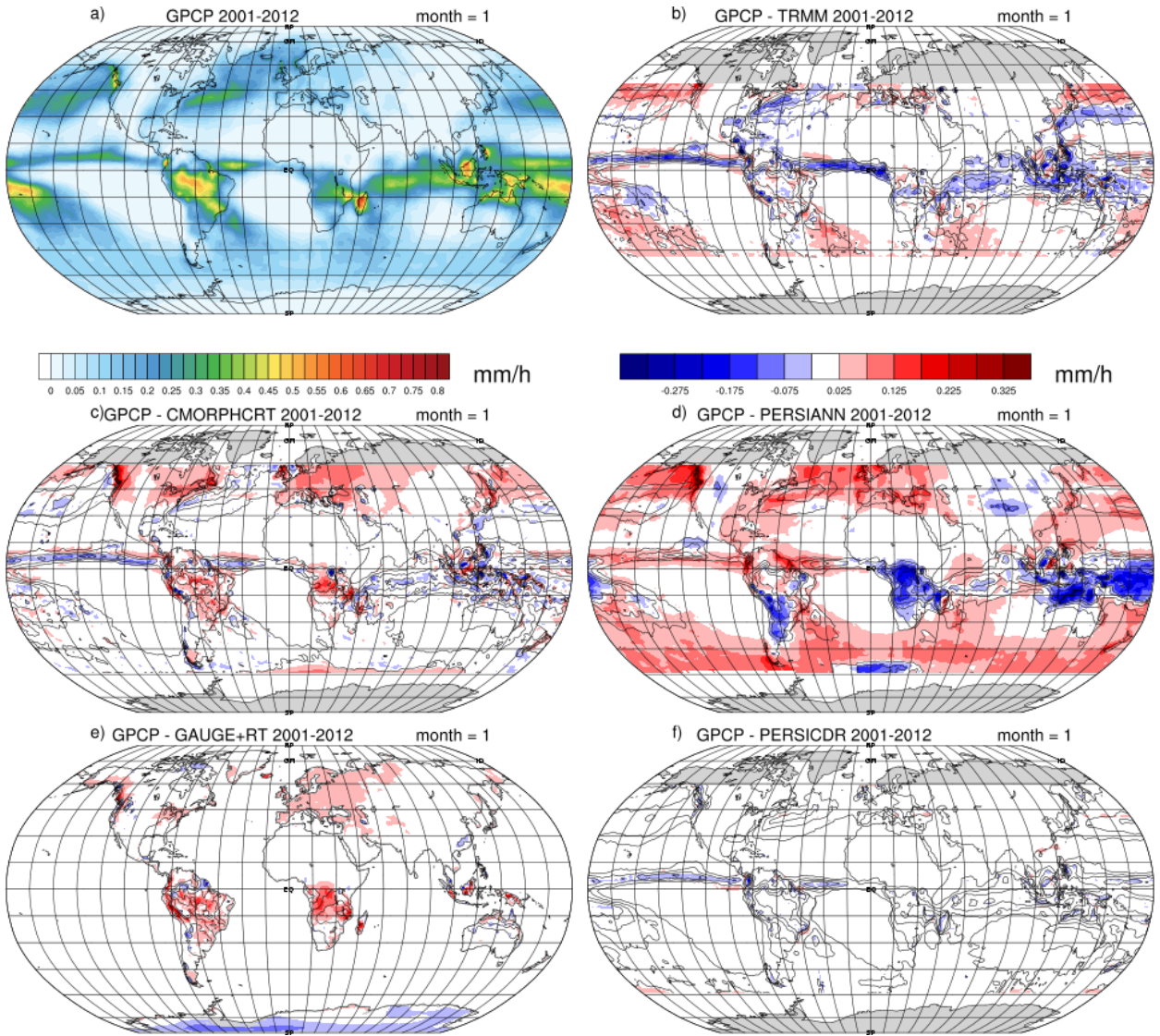
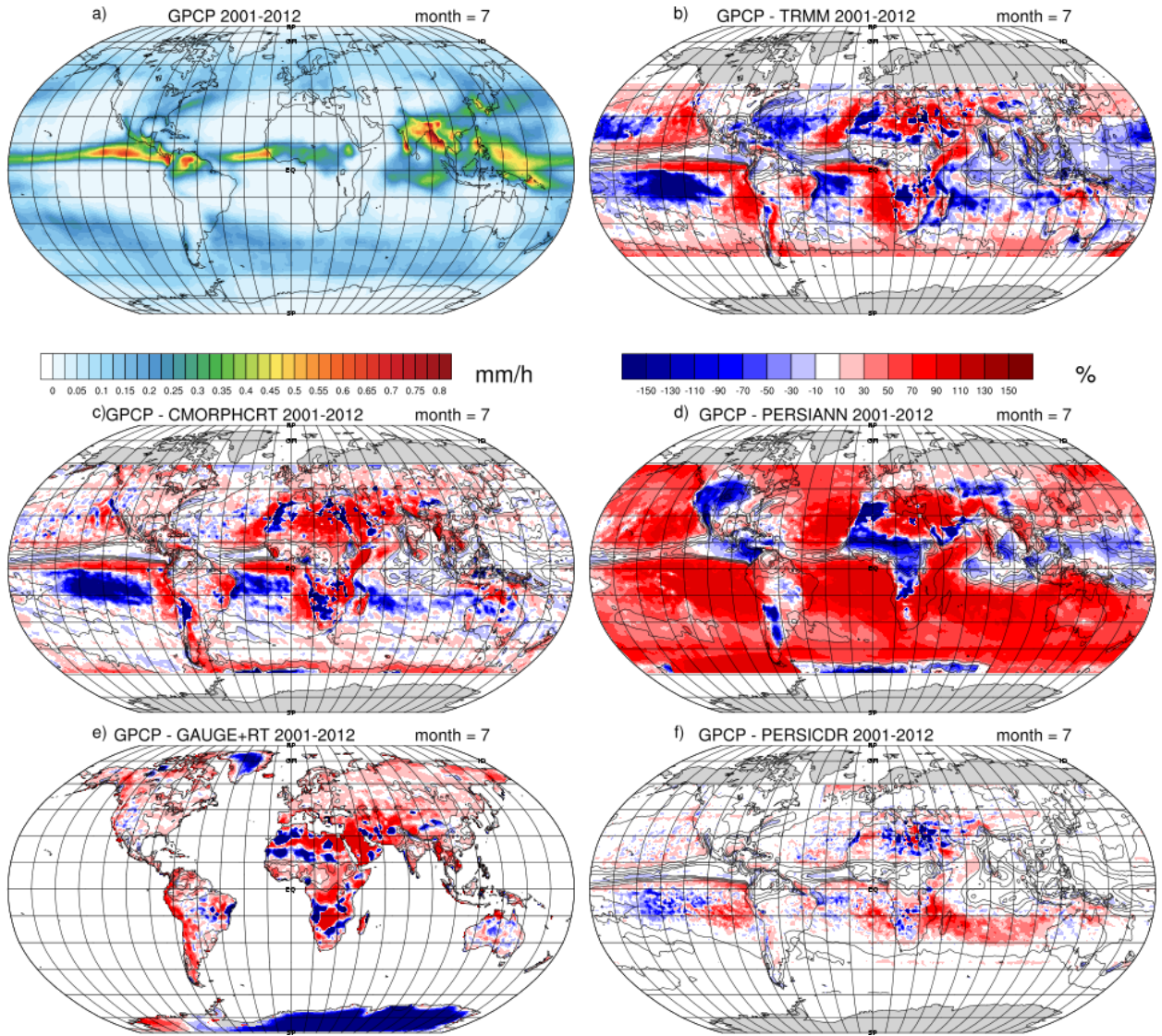
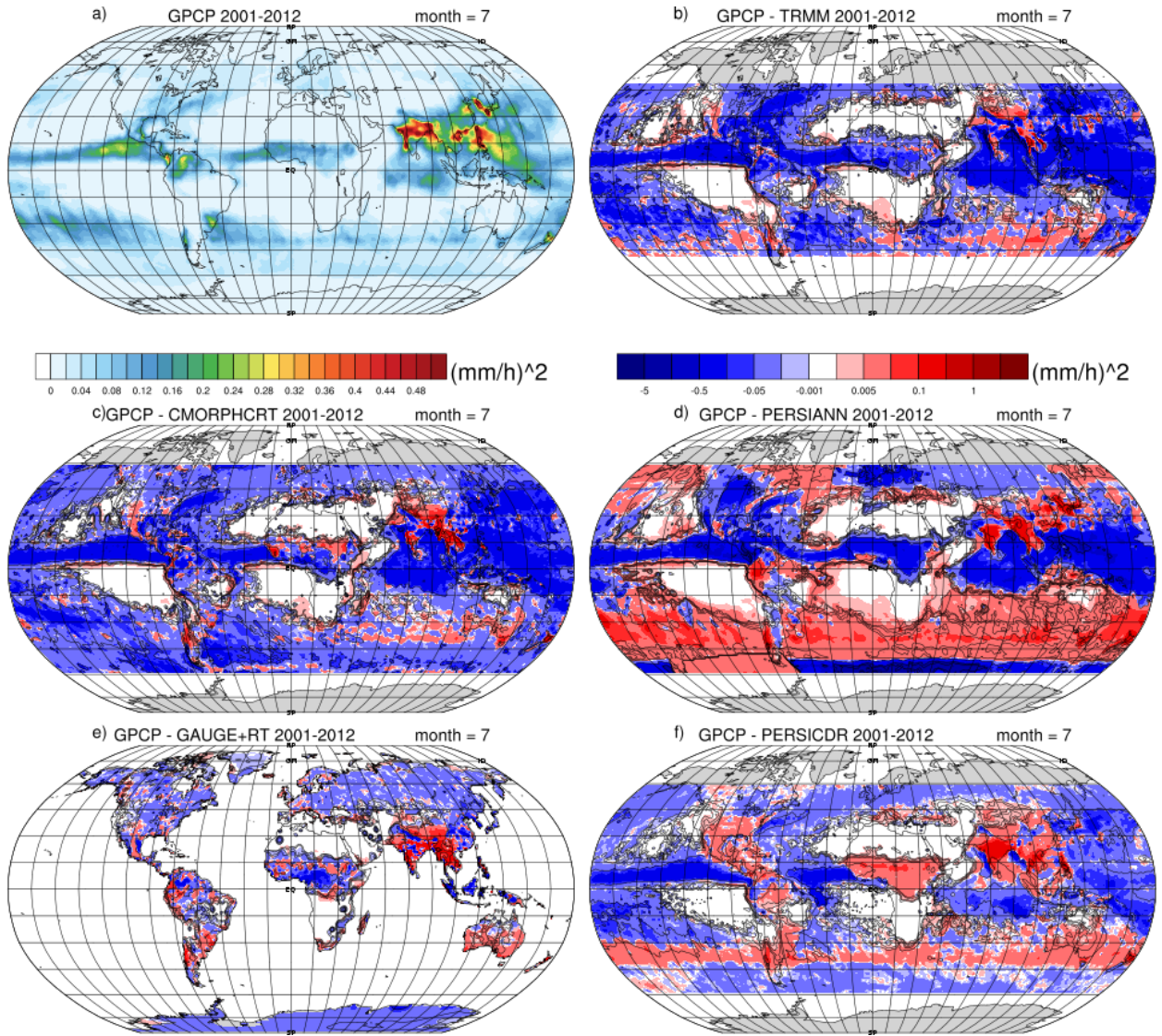


FIG. 5. Same as in Fig. 4, but for January.



892 FIG. 6. Monthly long term means of precipitation and percentage difference for July. a) mean for GPCP1DD.
 893 b)-f) the percentage difference between GPCP1DD mean and the respective data set mean for the period is
 894 indicated in shading, contours show the mean monthly precipitation for the respective data set. Contour levels
 895 as in Fig. 4.



896 FIG. 7. Monthly mean variance of precipitation for July. a) mean variance for GPCP1DD. b)-f) the difference
 897 between the GPCP1DD mean variance and the respective data set mean variance for the period is indicated in
 898 shading, contours show the mean monthly precipitation variance for the respective data set. Contour levels are
 899 (0.001,0.002,0.005,0.01,0.1,1,2,10).

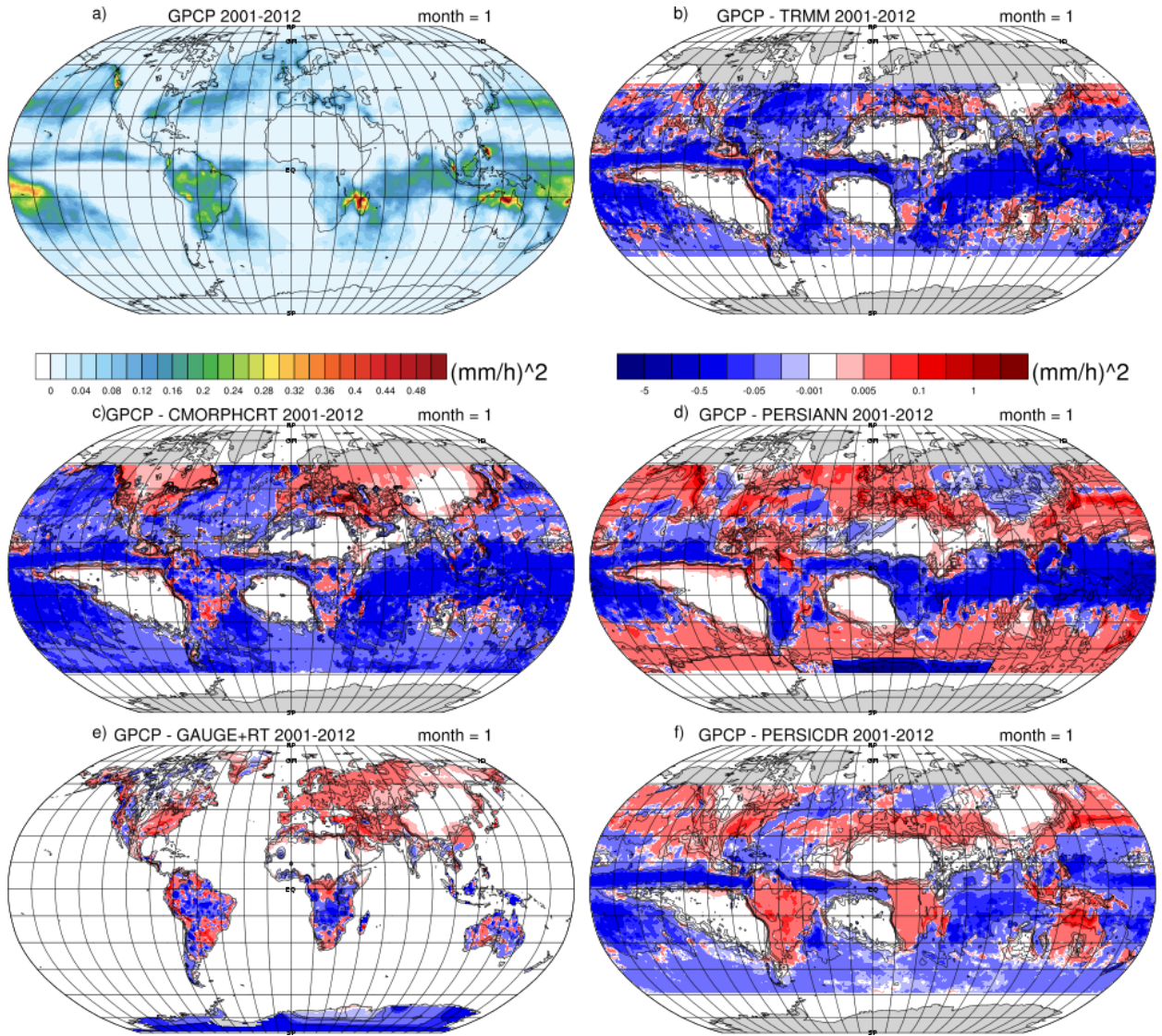
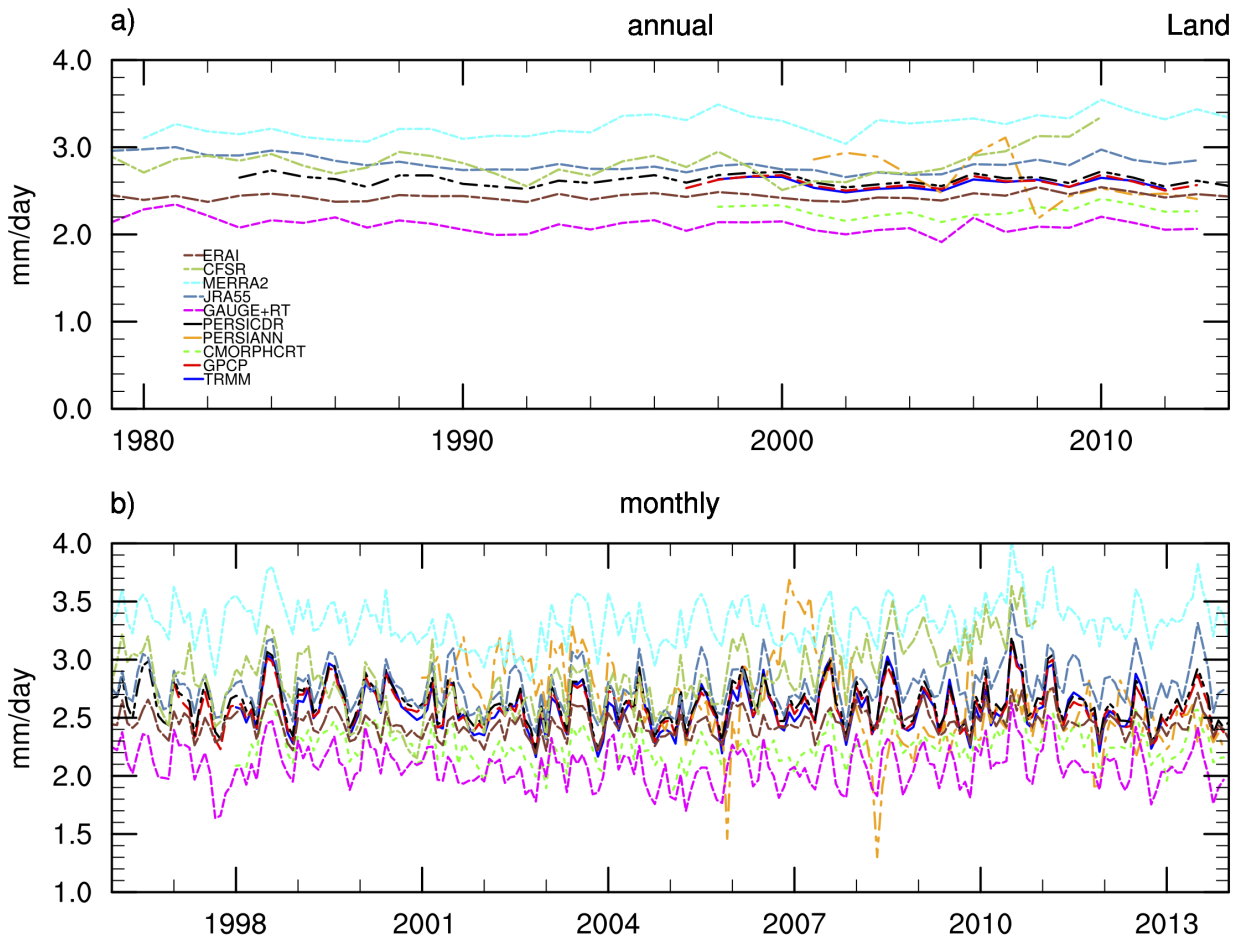
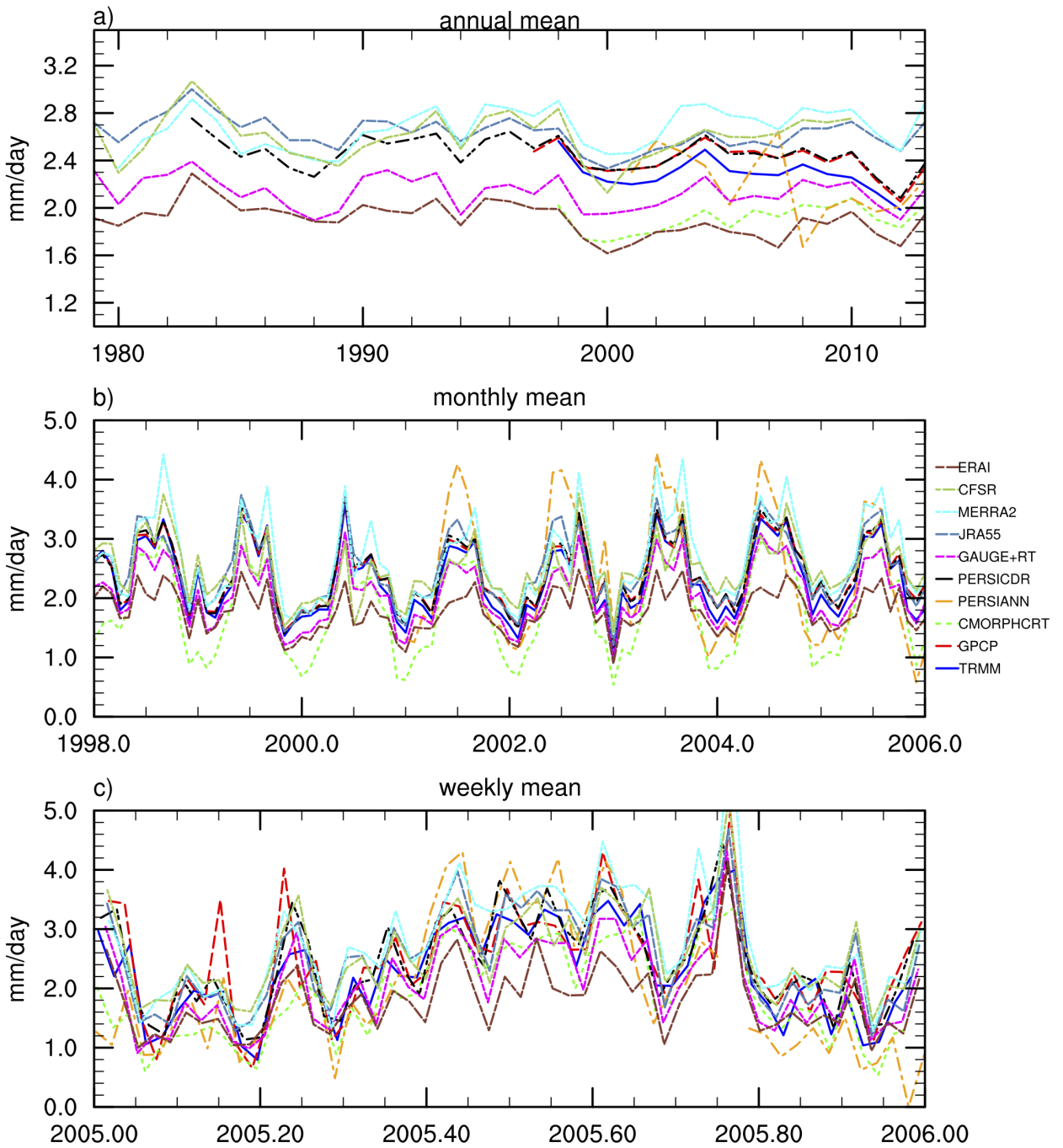


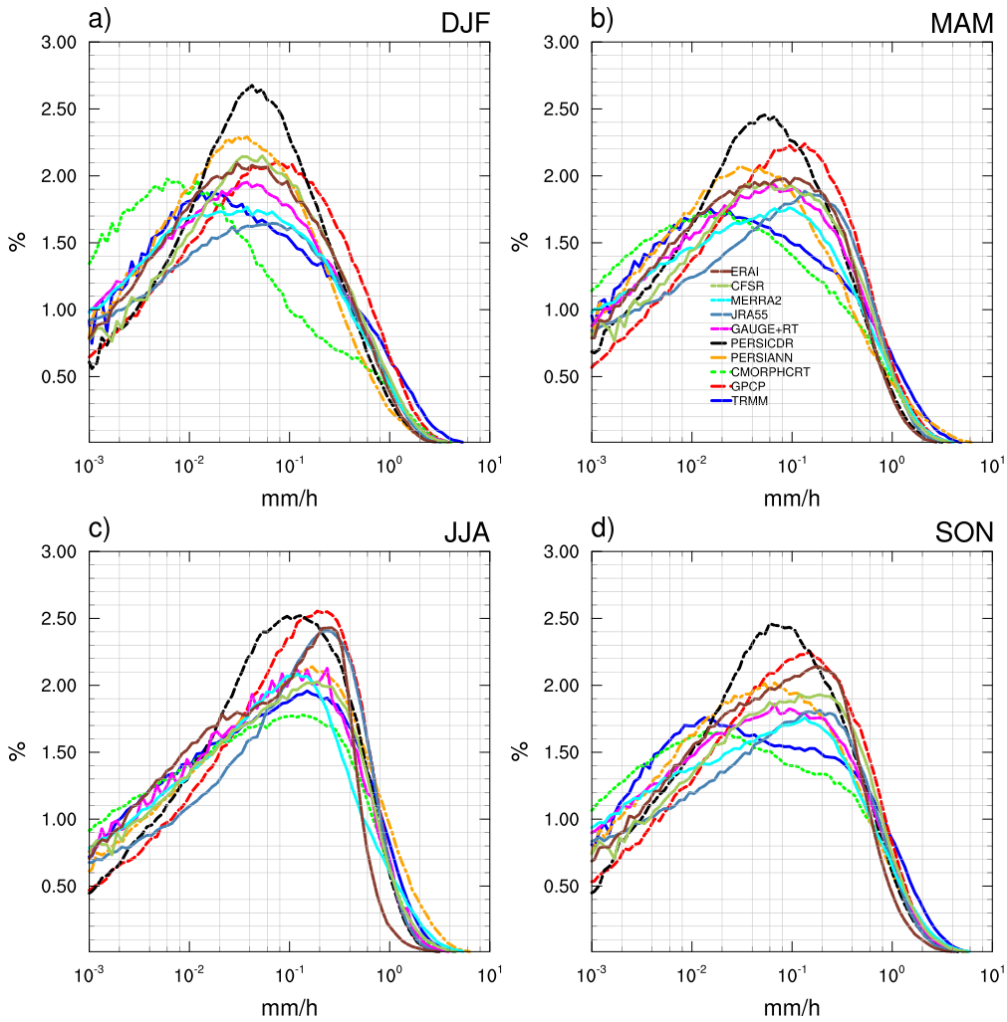
FIG. 8. Same as in Fig. 7, but for January.



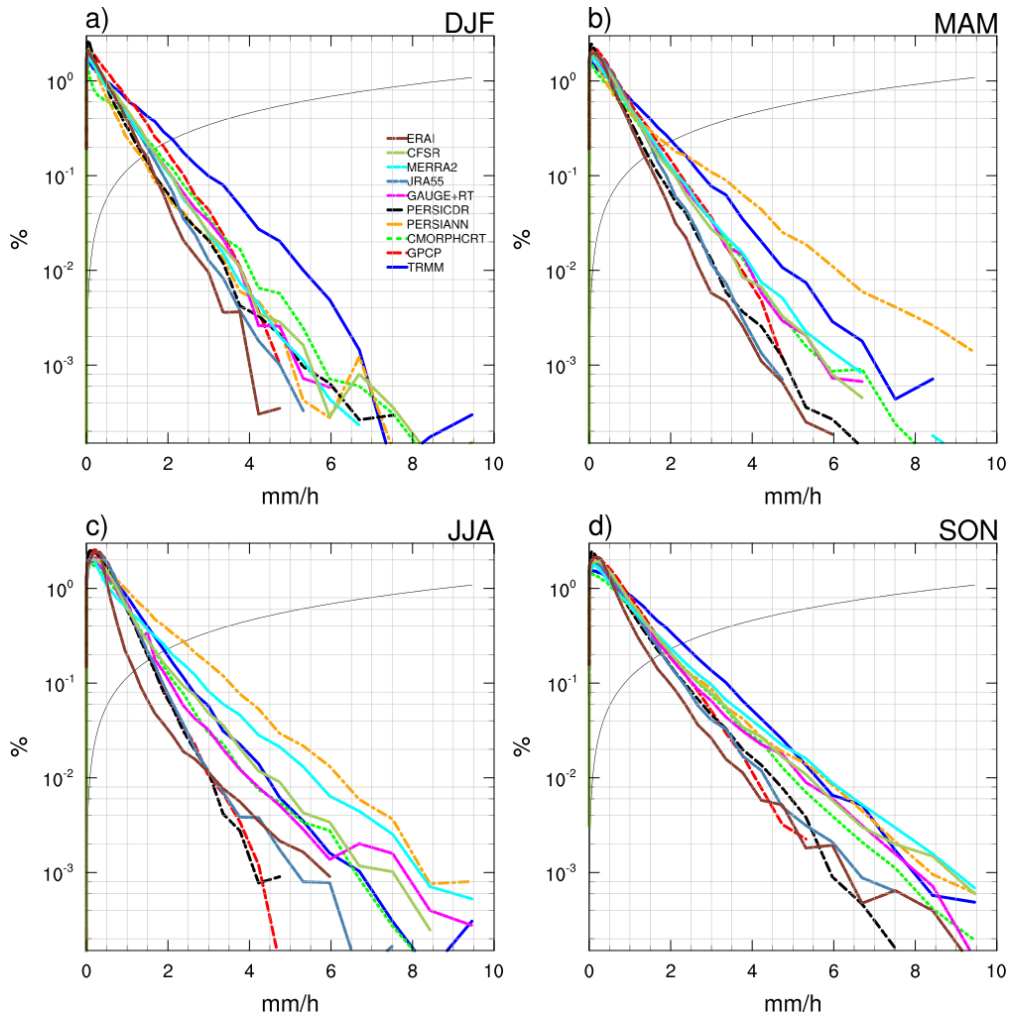
900 FIG. 9. Time series of rain rates averaged over global land area between 49°N and 49°S for a) annual means,
 901 and b) monthly means.



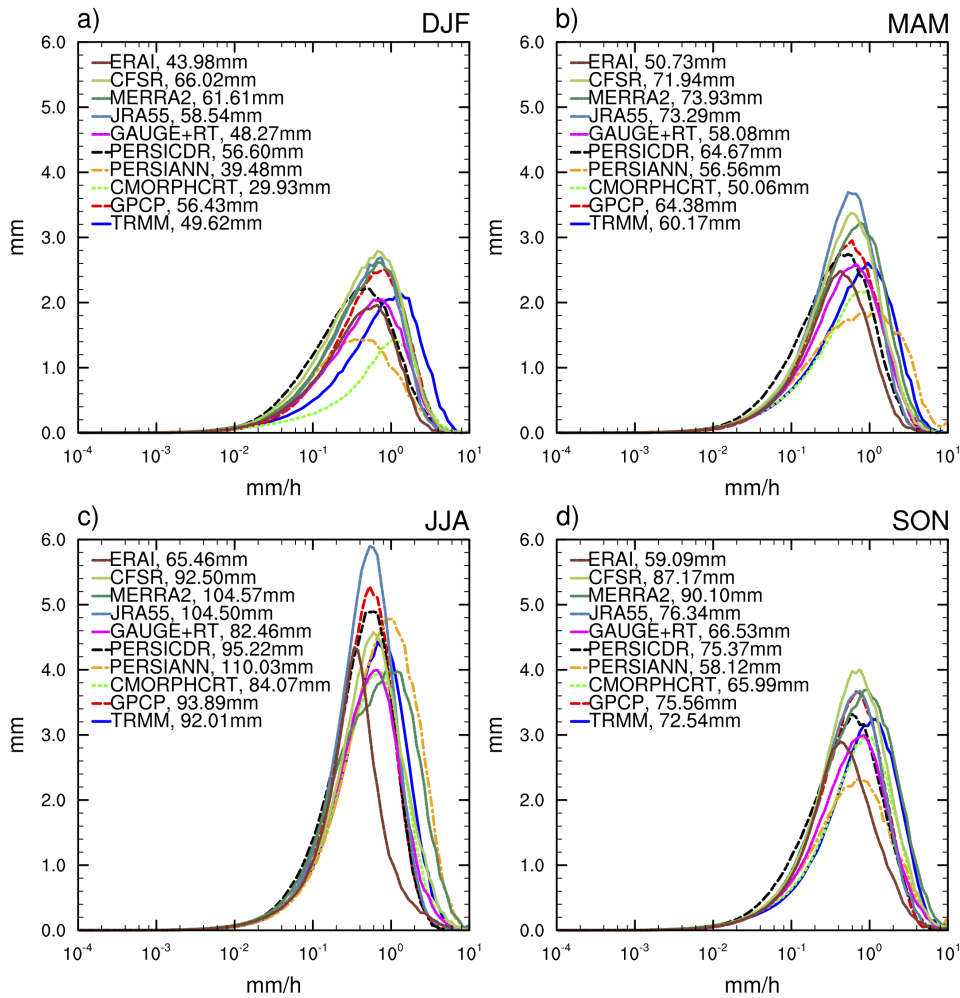
902 FIG. 10. Time series of rain rates averaged over North America land area between 15 – 49°N for a) annual
 903 means, b) monthly means, and c) weekly means.



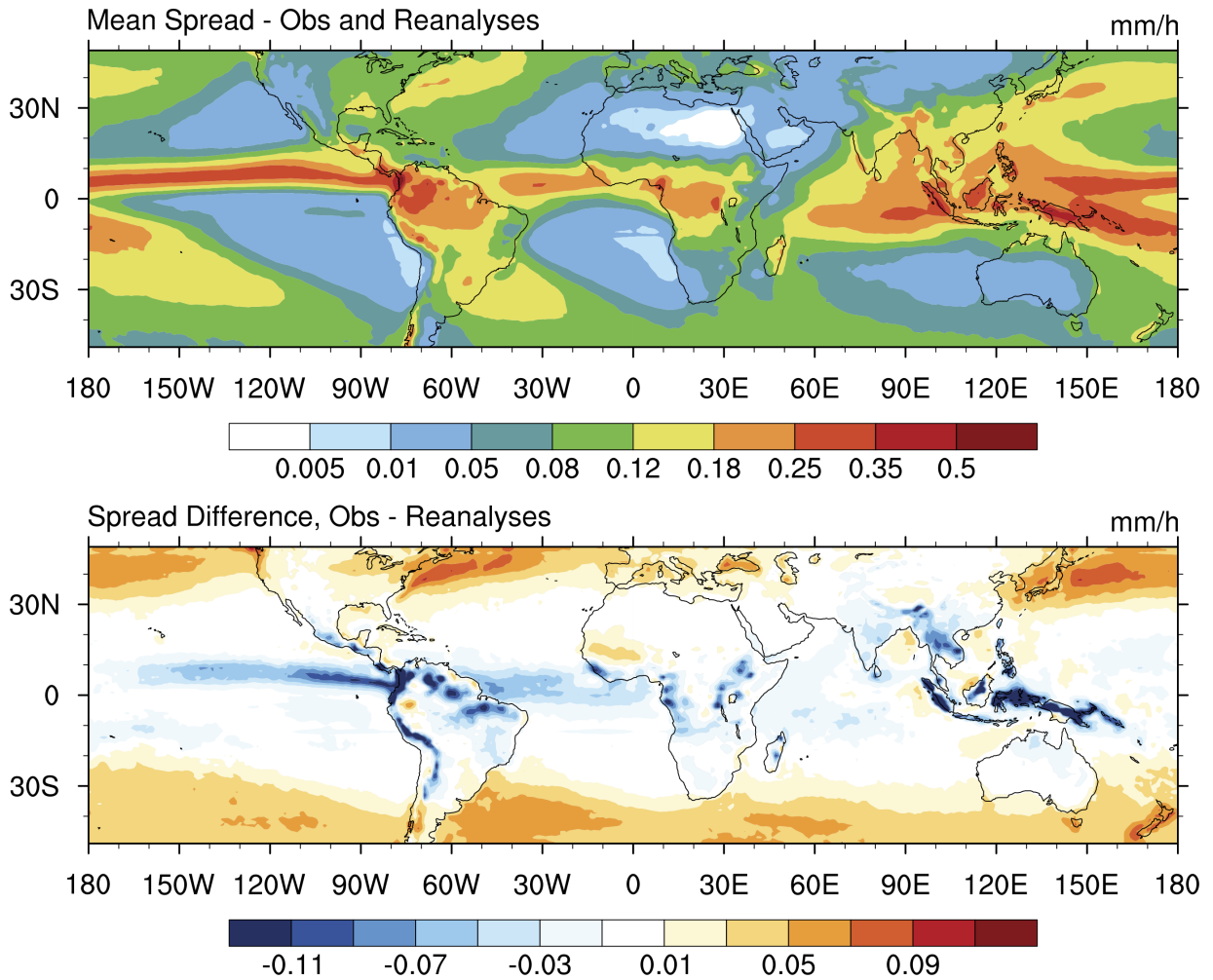
904 FIG. 11. Percentage distribution of precipitation rate over land area for North America ($15^{\circ}\text{N} - 49^{\circ}\text{N}$, 195°E
 905 $- 310^{\circ}\text{E}$). Panels a)-d) show the climatological distribution for all seasons for 2001 - 2012. Precipitation rates
 906 are binned with logarithmic bin sizes to account for more frequent rain events at low rain rates. The x axis is
 907 plotted on a log-scale and the y axis on a linear scale to compare the bulk of the distribution, not the tails. The
 908 black line shows the size of the bin at each precipitation rate. Distributions are computed for each month and
 909 grid point separately and then averaged over area and season.



910 FIG. 12. Percentage distribution of precipitation rate over land area for North America ($15^{\circ}\text{N} - 49^{\circ}\text{N}$, $195^{\circ}\text{E} -$
 911 310°E). As in Fig. 11, except that the x axis is plotted on a linear scale and the y axis on a log scale to facilitate
 912 comparison of the tails of the distributions.



913 FIG. 13. Distribution of precipitation amount by precipitation rate over land area for North America (15°N
 914 $- 49^{\circ}\text{N}$, the same area as is used in Fig. 10). Panels a)-d) show the precipitation amount distribution for all
 915 seasons for 2001 - 2012. The average is computed over the years 2001 - 2012. Insets show average monthly
 916 totals during each season for the different estimates.



917 FIG. 14. Spread among precipitation estimates (computed as the mean standard deviation among data sets) for
 918 2001-2010. Top panel: spread among precipitation data sets (including reanalyses). Bottom panel: difference
 919 in spread among observational precipitation data sets and spread among reanalyses. The mean seasonal cycle is
 920 removed from daily data prior to computing the spread.